1987-12

Development of a constituitive equation for HSLA-100 at cryogenic temperatures

Bissot, David M.

NAVAL POSTGRADUATE SCHOOL
Monterey, California

THESIS

Development of a Constituitive Equation for
HSLA-100 at Cryogenic Temperatures

by

David Michael Bissot

December 1987

Thesis Advisor: K. D. Challenger

Approved for public release; distribution is unlimited

SECURITY CLASSIFICATION OF THIS PAGE

REPORT DOCUMENTATION PAGE

1a. REPORT SECURITY CLASSIFICATION UNCLASSIFIED	1b RESTRICTIVE MARKINGS
2a SECURITY CLASSIFICATION AUTHORITY	3 DISTRIBUTION / AVAILABILITY OF REPORT Approved for public release; distribution is unlimited.
2b DECLASSIFICATION / DOWNGRADING SCHEDULE	
4 PERFORMING ORGANIZATION REPORT NUMBER(S)	5 MONITORING ORGANIZATION REPORT NUMBER(S)
6a NAME OF PERFORMING ORGANIZATION Naval Postgraduate School 6b OFFICE SYMBOL (*If applicable*) 69	7a NAME OF MONITORING ORGANIZATION Naval Postgraduate School
6c. ADDRESS (*City, State, and ZIP Code*) Monterey, California 93943-5000	7b. ADDRESS (*City, State, and ZIP Code*) Monterey, California 93943-5000
8a. NAME OF FUNDING / SPONSORING ORGANIZATION 8b. OFFICE SYMBOL (*If applicable*)	9. PROCUREMENT INSTRUMENT IDENTIFICATION NUMBER
8c. ADDRESS (*City, State, and ZIP Code*)	10. SOURCE OF FUNDING NUMBERS PROGRAM ELEMENT NO. / PROJECT NO / TASK NO / WORK UNIT ACCESSION NO

11 TITLE (*Include Security Classification*)
DEVELOPMENT OF A CONSTITUITIVE EQUATION FOR HSLA-100 AT CRYOGENIC TEMPERATURES

12. PERSONAL AUTHOR(S)
Bissot, David M.

13a. TYPE OF REPORT	13b TIME COVERED	14. DATE OF REPORT (*Year, Month, Day*)	15 PAGE COUNT
Master's Thesis	FROM _____ TO _____	1987 December	89

16. SUPPLEMENTARY NOTATION

17 COSATI CODES			18 SUBJECT TERMS (*Continue on reverse if necessary and identify by block number*)
FIELD	GROUP	SUB-GROUP	Voce equation, Power equation, Temperature dependence

19 ABSTRACT (*Continue on reverse if necessary and identify by block number*)

HSLA-100 is a 100ksi nominal yield strength steel being developed by the Navy for Naval shipbuilding applications. To assist in ductile and brittle failure modelling of this low carbon steel, tensile tests were conducted at temperatures ranging from 37 C(99 F)to liquid nitrogen(-196 C/-321 F)to determine a constituitive equation for this alloy at low temperature The Hollomon Power Equation and the Voce Equation are used to describe the true stress/true strain behavior to failure of individual tests. The Bridgman correction is applied to the true stress to compensate for the triaxial stress state that exists at and beyond the necking (maximum load) point. The power and Voce equations are then fit to the Bridgman corrected true stress versus true plastic strain. Relative comparisons are made between the two equations resulting in the conclusion that the Voce equation describes the stress-strain characteristics of this alloy better than the Hollomon equation. The temperature dependence of the material constants So, Si, and A, in the Voce equation were determined producing a constituitive equation for the tensile behavior of HSLA-100 as a function of strain and

20 DISTRIBUTION / AVAILABILITY OF ABSTRACT ☒ UNCLASSIFIED/UNLIMITED ☐ SAME AS RPT ☐ DTIC USERS	21 ABSTRACT SECURITY CLASSIFICATION UNCLASSIFIED
22a NAME OF RESPONSIBLE INDIVIDUAL K. D. Challenger	22b TELEPHONE (*Include Area Code*) (408) 646- 3036 22c OFFICE SYMBOL 69Ch

DD FORM 1473, 84 MAR 83 APR edition may be used until exhausted
All other editions are obsolete

SECURITY CLASSIFICATION OF THIS PAGE

U.S. Government Printing Office: 1986—606-24

(19. continued)
temperature, at a strain rate of about 1x10 -3 in/in sec. The Bridgman correction factorwas investigated in detail, mapping its change as a function of strain past the necking point. The Bridgman correction produced a discontinuity in the stress-strain curve at strains in the vicinity of the necking strain. This is not believed to be the true material behavior and thus, indicates that the Bridgman correction methodology is suspect.

Approved for public release; distribution is unlimited

Development of a Constituitive Equation for HSLA-100 at Cryogenic Temperatures

by

David M. Bissot
Lieutenant, United States Navy
B.S., United States Naval Academy, 1980

Submitted in partial fulfillment of the
requirements for the degree of

MASTER OF SCIENCE IN ENGINEERING SCIENCE

from the

NAVAL POSTGRADUATE SCHOOL
December 1987

ABSTRACT

HSLA-100 is a 100ksi nominal yield strength steel being developed by the Navy for Naval shipbuilding applications. To assist in ductile and brittle failure modelling of this low carbon steel, tensile tests were conducted at temperatures ranging from 37°C to liquid nitrogen (-196°C) to determine a constituitive equation for this alloy at low temperatures.

The Hollomon Power Equation ($\sigma = K\epsilon^n$) and the Voce Equation

($\sigma = \sigma_\infty - [\sigma_\infty - \sigma_o]\exp[-\epsilon/A]$) are used to describe the true stress / true strain behavior to failure of individual tests. The Bridgman correction is applied to the true stress to compensate for the triaxial stress state that exists at and beyond the necking (maximum load) point. The Power and Voce equations are then fit to the Bridgman corrected true stress versus true plastic strain. Relative comparisons are made between the two equations resulting in the conclusion that the Voce equation describes the stress-strain characteristics of this alloy better than the Hollomon equation.

The temperature dependence of the material constants, σ_o, σ_∞, and A, in the Voce equation were determined producing a constituitive equation for the tensile behavior of HSLA-100 as a function of strain and temperature, at a strain rate of about 1×10^{-3} in/in-sec. The Bridgman correction factor was investigated in detail, mapping its change as a function of strain past the necking point. The Bridgman correction produced a discontinuity in the stress-strain curve at strains in the vicinity of the necking strain. This is not believed to be the true material behavior and thus, indicates that the Bridgman correction methodology is suspect.

TABLE OF CONTENTS

LIST OF FIGURES 7

I. INTRODUCTION 9

A. CLASSIFICATION OF HSLA STEELS 9

B. DEVELOPMENT OF HSLA-100 10

C. PURPOSE AND SCOPE OF PRESENT WORK 12

II. BACKGROUND 14

A. TENSILE TESTING 14

B. STRESS STRAIN RELATIONSHIPS 18

1. The power equation 18

2. The Voce equation 19

C. CORRECTION FOR THE TRIAXIAL STRESS STATE IN THE NECK 21

D. TEMPERATURE EFFECTS ON MATERIAL BEHAVIOR 22

III. EXPERIMENTAL PROCEDURE 23

A. MATERIAL AND SAMPLE PREPARATION 23

B. TEST APPARATUS 26

C. DATA COLLECTION AND REDUCTION 29

IV. ANALYSIS AND RESULTS 31

A. DETERMINATION OF THE ELASTIC MODULUS 31

B. INITIAL TESTING AND ANALYSIS OF HOURGLASS SAMPLES 31

1. Computer aided determination of the Voce coefficients 32

2. Modifications to the testing procedure 35

C. COMPLETION OF TESTING HOURGLASS SPECIMENS 35

1. Voce coefficients and comparison to the Hollomon power equation 36

2. The Voce equation as a function of temperature 42

D. BRIDGMAN CORRECTED TRUE STRESS VERSUS TRUE PLASTIC STRAIN 51

E. MECHANICAL PROPERTIES OF HSLA-100 WITH TEMPERATURE 54

1. 0.2 percent offset yield strength 54

2. Ductility 56

3. Ultimate tensile strength 56

F. FRACTURE CHARACTERISTICS AND METALLOGRAPHY 58

V. DISCUSSION 68

A. MODIFICATIONS / IMPROVEMENTS IN THE USE OF THE VOCE EQUATION 68

B. SAMPLE GEOMETRY RELATIONSHIP TO FRACTURE 70

VI. CONCLUSIONS AND RECOMMENDATIONS 73

APPENDIX A: INTERIM SPECIFICATION FOR TRIAL COMMERCIAL PRODUCTION OF HSLA-100 STEEL PLATES 75

APPENDIX B: BASIC COMPUTER PROGRAM FOR CALCULATION OF VOCE EQUATION COEFFICIENTS 78

APPENDIX C: BASIC COMPUTER PROGRAM FOR FITTING AN EXPONENTIAL FUNCTION 84

LIST OF REFERENCES 87

INITIAL DISTRIBUTION LIST 88

LIST OF FIGURES

1. Typical load / displacement curve 14
2. Typical true stress - true strain curve 16
3. Typical logarithmic stress - strain curve 17
4. Light micrograph of aged HSLA-100, 2 percent nital etch for 25 seconds 25
5. TEM micrograph of aged HSLA-100 25
6. Tensile specimen drawings 27
7. MTS function generator, controls and test assembly 28
8. Environmental test chamber, actuator and grips 29
9. Data acquisition system 30
10. Determination of S_∞ and the characteristic strain 33
11. Estimate of the Voce equation and failure point - Sample number 36 34
12. Typical experimental load/displacement and true stress/true strain plots 37
13. Comparison of the Voce and power equations 41
14. Voce stress coefficients as a function of temperature (1) 43
15. Characteristic strain as a function of temperature 44
16. Voce(T, ϵ) - Plots of two tests 46
17. Voce stress coefficients as a function of temperature (2) 47
18. Final Voce (ϵ, T) comparison plots 49
19. Collection of all Bridgman correction data points for HSLA-100 tests 53
20. Bridgman corrected true stress versus true plastic strain plots 55
21. 0.2 percent offset yield strength 57
22. Ductility of HSLA-100 57

23. HSLA-100 ultimate tensile strength....58
24. HSLA-100 sample 19 (-117°C) vertical split....60
25. HSLA-100 sample 52 (-170°C) cross section of neck....60
26. Fracture profiles....61
27(a). Sample 30 (0°C) fracture surface, low magnification....63
27(b). Sample 51 (-30°C) fracture surface, low magnification....63
27(c). Sample 30 (0°C) fracture surface, high magnification....64
27(d). Sample 20 (-71°C) fracture surface, low magnification....64
27(e). Sample 23 (-101°C) fracture surface, low magnification....65
27(f). Sample 23 (-101°C) fracture surface, high magnification....65
27(g). Sample 26 (-140°C) fracture surface, low magnification....66
27(h). Sample 47 (-150°C) fracture surface, low magnification....66
27(i). Sample 52 (-170°C) fracture surface, high magnification....67
28. Prediction of the ultimate tensile strength....70
29. Two curve fit for the Bridgman corrected true stress/true plastic strain....71

I. INTRODUCTION

A. CLASSIFICATION OF HSLA STEELS

The term HSLA, High-Strength Low-Alloy, is used to characterize a broad spectrum of steels which may have widely varying chemical compositions and mechanical properties. HSLA steels generally have higher yield strengths than plain carbon structural steels and may also show varying amounts of other beneficial properties such as: greater fracture toughness, formability, weldability, and good atmospheric corrosion resistance [Ref. 1]. Several categories of HSLA steels include: weathering steels, control-rolled steels, pearlite-reduced steels, microalloyed steels, acicular ferrite steels, and dual phase steels [Refs. 1, 2: p. 4•50].

Microalloying in the HSLA steels is capable of producing many characteristics desired for naval shipbuilding applications. The very low carbon content in some of these steels in conjunction with niobium reduces the formation of iron carbides and instead form niobium carbonitrides during hot rolling. The carbonitrides retard grain growth, providing grain refinement, increasing strength and toughness without increasing the ductile-to-brittle transition temperature (DBTT)[Refs. 1, 3]. Molybdenum increases the aged strength of the steel, improves toughness , and hardenability while reducing grain boundary segregation[Ref. 4].

Copper in concentrations of greater than 0.75 percent increases the aged strength of HSLA steels. On aging at temperatures over 500°C (930°F) coherent body centered cubic clusters of copper form, precipitation hardening the steel. On continued or subsequent aging these coherent particles transform into non-coherent ϵ-phase Cu particles. At the point of

maximum strength only a few particles are visible under an electron microscope [Refs. 3, 5]. They are hard to "see" because they are coherent. The particle size at maximum strength has been shown to be 50 angstroms. Copper is also the element responsible for increasing the steels atmospheric corrosion resistance.

Problems associated with copper as an alloying element are related to its relatively low melting temperature, 1083°C (1981°F) for Cu versus 1536°C (2798°F) for Fe. This becomes a problem when solution heat treating a copper precipitated steel or when hot-working the steel at a temperatures above 1050°C (1922°F) with copper concentrations above 0.5 percent. Copper builds up in steel scrap and cannot be removed in subsequent steel production heats creating further difficulties in reprocessing. Nickel is added to the steel to prevent the molten copper from penetrating the austenite grain boundaries (hot-shortness). [Refs. 3, 5]

One of the major beneficial qualities of HSLA steels is its weldability without any pre-heating, due primarily to the low carbon content of the steels. Some of the weld metal / heat affected zone (HAZ) characteristics include good ductility and toughness without significant losses in strength compared to the base metal. [Refs. 1, 6]

B. DEVELOPMENT OF HSLA-100

Weld preparation is a very high cost and time consuming process in naval ship construction. The HY series of steels exhibit both the required strength and toughness in base metal and welds but entail detailed and expensive welding procedures. An already qualified, low carbon, copper precipitation strengthened, HSLA-80 steel showed excellent weld strength and toughness without any preheat in plates less than 3/4 inch thick. To expand on the capabilities demonstrated by this steel, a research program funded under the

SSN-21 project was initiated by the Naval Sea Systems Command and David Taylor Naval Ship Research and Development Center. This project was completed under contract to the AMAX Materials Research Center (AMRC), subcontracted to Phoenix Steel Corporation, Claymont Delaware. [Ref. 7]

The purpose of the development project was to modify the current HSLA-80 steel into a highly weldable, copper precipitation strengthened steel, with carbon content less than 0.07 percent , sulfur less than 0.008 percent, phosphorous less than 0.010 percent, containing manganese, nickel, chromium, and molybdenum. In addition the steel was required to be solution treated, quenched and aged with a nominal 0.2 percent offset yield strength ranging between 100 ksi (689 MPa) and 120 ksi (827 MPa), minimum average transverse Charpy V-notch impact properties of 55 ft-lb (75 J) at 0°F (-18°C) and 30 ft-lb (41 J) at -120°F (-84°C), minimum elongation of 18 percent in 2 inches (51 mm), and minimum reduction in area of 45 percent. These requirements dictate that strengthening from solid solution, grain refinement, and precipitation must be present. [Ref. 7]

Three phases of development for the new steel were defined by: laboratory development of prospective compositions and heat treatments (Phase I), production and testing of a trial commercial heat (Phase II), and procurement of a larger quantity of steel (Phase III) based on the results of testing of the Phase II steel. The resultant, interim, specifications for a HSLA-100 trial heat were as specified in Appendix A. [Ref. 7]

The microstructure of the selected steel is a 100 percent low-carbon banite with large amounts of copper (1.6 percent) and nickel (3.5 percent) for strength and toughness. Minimal quantities of niobium are for austenite grain size control. [Ref. 7]

Sensitivity to quenching from the solution treating temperature was found to be a concern only in plates greater than one inch. The effect of a slow quench possibly caused by

an overheated quenching media would be inadequate retention of copper in solid solution and lower yield strengths. The 100 percent banite microstructure was producible with even the slowest quenches used during the development. [Ref. 7]

C. PURPOSE AND SCOPE OF PRESENT WORK

Brittle fracture is type of failure characterized by rapid crack propagation and little or no associated plastic deformation. There is a generally high tensile stress and lower energy associated with this type of fracture initiation when compared to ductile fractures. Ductile fracture is characterized by microvoid initiation, growth, and coalescence, resulting typically in a cup and cone morphology. Initiation sites have been associated with decohesion of carbides or inclusions. [Ref. 8]

The type of fracture, brittle or ductile, depends on many variables such as chemical composition (alloying) and processing of the steel. Other dependent variables include the section size, strain rate, and the temperature at which the test was conducted. Higher temperatures are generally associated with ductile fractures and lower temperatures with brittle fractures. There is a temperature range associated with the transition from ductile to brittle type fractures, denoted by a temperature called the ductile to brittle transition temperature (DBTT). [Ref. 8]

There are several models used to describe crack initiation and propagation for cleavage fractures but they rely heavily upon iron carbides as crack initiation sites. HSLA-100 contains very low levels of carbon and these models have difficulty describing initiation of cleavage in the upper transition temperature regions. To better understand and model the toughness behavior of HSLA-100 and future steels a program is in progress to investigate the micromechanics of HSLA-100 fracture behavior. In the first of three stages of this project one of the requirements is to derive true stress / true strain tensile curves as a

function of temperature which will provide the necessary rheological input for a finite element analysis of HSLA-100. The purpose of this research to derive this constituitive equation of the stress as a function of strain and temperature under the conditions of a quasi-static deformation. [Ref. 8]

II. BACKGROUND

A. TENSILE TESTING

The data obtained in a tensile test is generally load, measured by a load cell or some other means, and displacement, measured by an extensometer or crosshead movement. When plotted in typical fashion with load plotted on the ordinate (Y-axis) and displacement on the abscissa (X-axis) the general form of the curve is as shown in Figure 1.

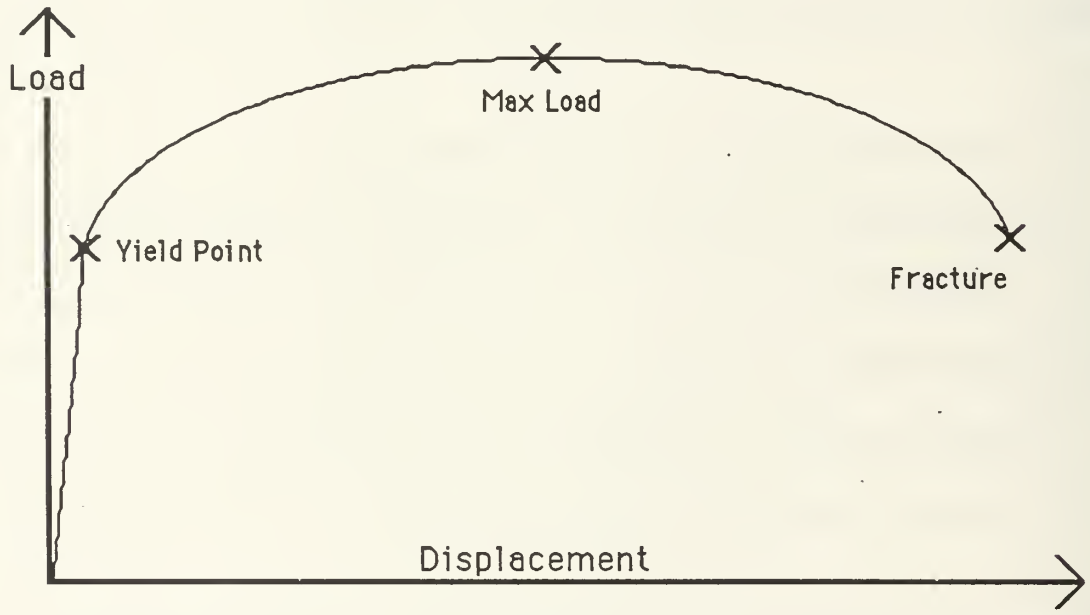

Figure 1.
Typical Load/Displacement Curve

In this Figure there are three important points. First is the yield point where the curve deviates from the initial approximately linear portion of the curve. The point of maximum load is the second, where necking begins and corrections for the triaxial stress state at the minimum diameter begins. The curve from this point shows a decreasing load carrying ability as displacement continues, until fracture when the specimen incapable of carrying any load. [Ref. 9: pp. 13-15]

Conversion of the load into true stress and displacement into true strain results in a more usable form of the information for engineering purposes. True stress is calculated by the equation:

$$\sigma_T = F_i/A_i$$

where F_i is the instantaneous load carried by the specimen, and A_i is the instantaneous cross-sectional area of the specimen. The true stress, σ_T, describes the state of stress, in units of force/unit area, in the plane where that cross sectional area was measured.

A fundamental assumption associated with calculating the true strain is that the volume of the sample remains constant throughout the deformation. With this, volume, V= constant= $A_i\ l_i = A_o\ l_o$, where l_i is the instantaneous length and the subscript 'o' denotes the initial conditions. True strain is defined as:

$$\epsilon_T = \mathrm{Ln}(A_o/A_i) = \mathrm{Ln}(l_i/l_o) = 2\ \mathrm{Ln}(d_o/d_i)$$

A typical true stress-true strain curve is diagrammed in Figure 2.

In this curve the section from the origin to point A is the elastic portion of the curve. The elastic portion of the stress-strain curve is nearly linear and thus the stress strain ratio should be a constant. This ratio was initially described by Robert Hooke in 1678 and bears his name, Hooke's law [Ref. 10: p. 6].

$$E = \sigma/\epsilon\ .$$

In this equation the constant E, called Young's modulus, is one of the fundamental constants describing the stiffness of the material. To define the yield point, frequently a difficult point to specify exactly, another commonly used property is defined as the 0.2 percent offset

yield strength. To arrive at the 0.2 percent offset yield strength a line is drawn parallel to the elastic portion of the stress-strain curve, slope equal to E, intersecting the X-axis at 0.2 percent strain. Where the line crosses the stress / strain curve defines the 0.2 percent offset yield strength.

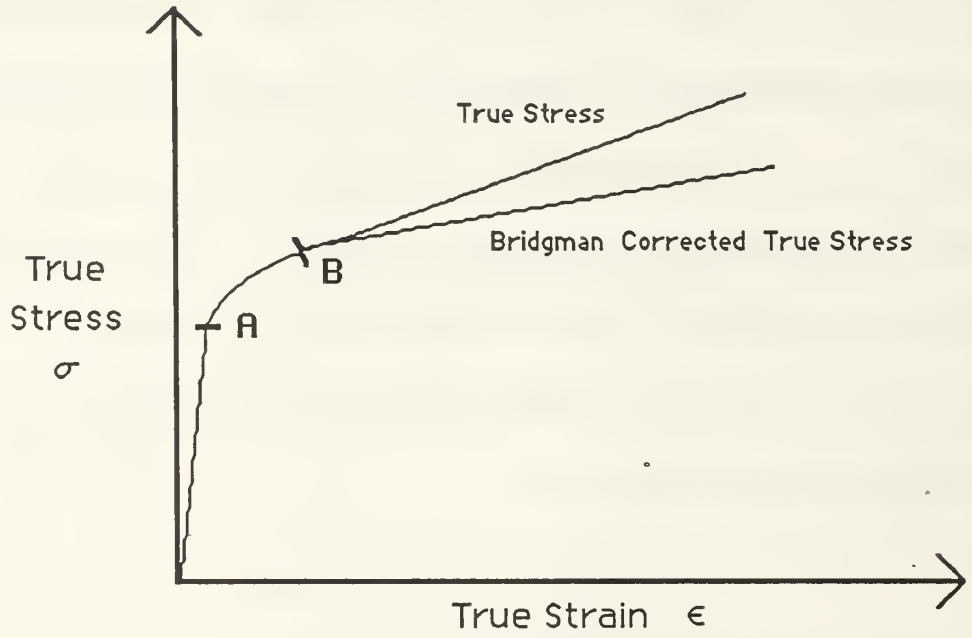

Figure 2.
Typical True Stress-True Strain Curve

The second portion of the curve, from point A to B, is the region of uniform plastic deformation and generally follows an equation of the form:

$$\epsilon^n = \sigma/K.$$

The final portion of the stress-strain curve, from point B to failure, is called the region of non-uniform plastic deformation and once again strain is approximately proportional to stress. The lower curve shown in Figure 2 describes the stress corrected for the triaxial stress state which exists in the neck. This will be discussed in more detail later. [Ref. 9: pp 13-17]

In the latter two portions of the curve there are two strain hardening regimes. Strain hardening is the phenomenon whereby a material strained past the yield point, when relaxed will follow a line approximately parallel to the elastic portion of the curve and when retensioned will begin to yield at a load higher than the initial yield point. The difference in the yield points is the strain hardening and the amount of strain not recovered during relaxation is the plastic deformation. Expressing mathematically the plastic deformation as a strain, the plastic strain, ϵ_p, is :

$$\epsilon_p = \epsilon_t - (\sigma/E)$$

where the quantity σ/E is the elastic strain of the material. [Ref. 9: pp. 15-17]

When these stress-strain points are plotted on logarithmic coordinates the shape of the curve will often be a shallow S-shape as shown in Figure 3.

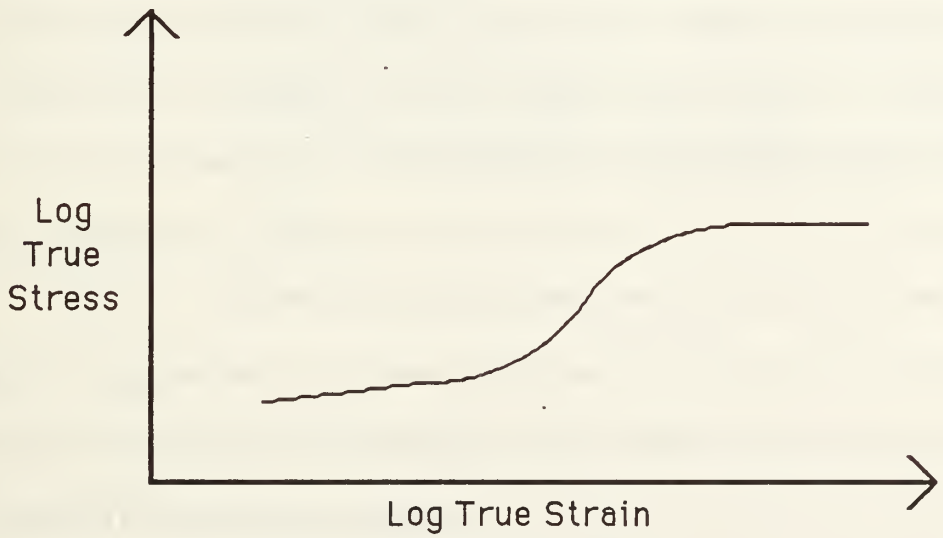

Figure 3.
Typical Logarithmic Stress-Strain Curve

This form of the stress-strain curve is the basis of two stress-strain relationships which will be discussed in more detail.

B. STRESS STRAIN RELATIONSHIPS

Over the years many forms of stress-strain relations have been formulated. Two which have gained some recognition are the Power Equation and the Voce equation.

1. The Power Equation

The power equation, attributed to Ludwik (1909) ($\sigma = \sigma_o + K\epsilon^n$) and Hollomon (1945) ($\sigma = K\epsilon^n$), were widely used for many years to describe stress-strain behavior. When the logarithmic plot of the stress-strain curve is viewed on some scales, a straight line appears to fit the curve very well through all portions of the curve. The Hollomon version of the equation is more widely used and may take either of the forms:

$$\sigma = K\epsilon^m \quad \text{or:}$$

$$\log \sigma = \log K + m \log \epsilon.$$

K is called the strength coefficient and represents the true stress at a unit true strain. The quantity log K is the least squares Y-intercept of the straight line representation of the curve. The slope of the line, m, is the slope of the line on logarithmic coordinates and represents the strain hardening rate. It is mathematically equal to the true strain at the necking point (maximum load). The coefficients for this equation are affected by variables of testing including temperature and strain rate. [Ref. 11: pp 155-156]

This equation has been shown to have limited success in describing stress-strain data beyond the point of necking (maximum load). This equation is more successful when used with true plastic strain instead of the true strain. Because of the simplicity of the power equation it is good for fast comparisons of materials. The solution of the coefficients can be easily determined by a least squares linear curve fit of logarithmic stress-strain data points. The slope of the line is the strain hardening coefficient and the intercept is equal to

the log of the strength coefficient. [Refs. 10: pp 373-375, 11: pp155-156]

2. The Voce equation

Voce disagreed with the form of the power equation because of its empirical nature and its failure to accurately describe the S-shaped form of logarithmic stress-strain curve. In addition, the power equation implies that load carrying ability or strain hardening would infinitely increase as the material is deformed. What is seen experimentally is a leveling off at some value for incremental increases in strain. [Ref. 11: pp.160-169, 12]

To arrive at a different form of an equation describing the stress-strain curve Voce looked at the logarithmic curve for copper samples and picked the approximately asymptotic values at small and large strains. Several terms Voce used in his equation and some alternate forms of them follow:

TABLE 1 SYMBOLOGY USED WITH THE VOCE EQUATION

Primary	Alternate	Definition
S_o	σ_o	The initial or threshold stress where homogeneous plastic deformation begins.
S_∞	σ_∞	The final constant stress at which deformation proceeds without an increase in stress.
Q_b		Equal to (S_∞ - So), the plastic stress capacity of the material.
C		Equal to (S_∞ -S), the plastic stress remaining in the material.
R		The strain ratio, equal to l/lo = Ao/A = $(do/d)^2$ in tension testing. Ln R= ϵ.
A	ϵ_c, k	A constant called the characteristic strain.

In his analysis of copper samples in compression he noted that a plot of the strain versus Ln(C/Co) resulted in a linear plot. By rearranging the terms and solving for stress he arrived at the final form of the Voce equation:

$$S = S_\infty - (S_\infty - S_o)\, e^{-\epsilon/A}$$

This form of the equation has equal or better results in fitting stress-strain data than the power equation and in most cases is applicable for tensile tests as well as compressive tests.

It can be used for any material showing the characteristic curve shown in Figure 3. A problem associated with the use of this equation is that it is most accurate at high strains thus does not accurately describe the elastic portion of the stress-strain curve and may fit poorly in the region of uniform plastic deformation. [Refs. 11: 160-162, 12]

The Voce model does have some physical reality (thus not purely empirical). For example, if there is some finite number of strain hardening sites and a small increment of strain is applied to the material, a small portion of the strain hardening sites will be blocked. This proportion of the blocked sites to the total number of hardening regions is equal to the proportion of the plastic stress capacity used in the material as compared to the total plastic stress capacity of the material:

$$\frac{n}{N} = \frac{(S - So)}{(S\infty - S)}$$

Viewed from a dislocation movement point of view, the initial asymptotic portion of the curve exists because dislocations are free to move with none, or very few being blocked. As deformation proceeds an increasing amount of the dislocations become blocked until finally the stress asymptotically approaches $S\infty$ because the blockage rate and annihilation rate of dislocations balance. [Refs. 11: pp. 164-165, 12]

In the treatment of specimens which have some unknown degree of plastic deformation in them, the power equation is incapable of detecting the initial strain hardening associated with it. If the Voce equation coefficients are known for the material, the amount of prestrain on the material can be predicted accurately from the point where the prestrained specimen meets the original Voce curve, The value of A, and $S\infty$ will remain unchanged. [Ref 11: p. 171]

C. CORRECTION FOR THE TRIAXIAL STRESS STATE IN THE NECK

The maximum load point of the load-displacement curve is the point where necking begins. The axial stress state in the neck and the load measured by the load cell are not equal because of a radial component of flow for material in the vicinity of the neck of a cylindrical sample. The physicist, Percy Williams Bridgman, studied on this problem. In his analysis of the true axial stress in the neck of a tensile specimen he used tensors in cylindrical coordinates, equilibrium and boundary conditions (compatibility) at the surface as a start point in the analysis. The round tensile samples are assumed to have rotational symmetry and picking the origin at the minimum diameter or the sample, there is assumed to be symmetry on the $\pm$ z-axis. Applying the von Mises criterion of maximum distortion energy to the stresses he was able to arrive at an equation which approximates the actual uniaxial stress state in the neck.

$$\sigma = \sigma_{av} / (1 + 4R/d)\ \mathrm{Ln}(1 + d/4R)$$

In this equation, σ is the stress corrected for the triaxial stresses in the neck and is always less than the stress measured by the load cell (divided by the area). The measured stress is σ_{av}, R is the radius of curvature in the vicinity of the minimum diameter of the neck, and d is the minimum diameter of the neck. The quantity , $1 / (1 + 4R/d)\ \mathrm{Ln}(1 + d/4R)$, is equal to σ / σ_{av} and is the Bridgman correction [Refs. 10: pp. 566-569, 13].

In an attempt to generate an empirical relation of the Bridgman correction to more readily obtained stress-strain information Bridgman and others had some success in correlating the Bridgman correction to the true strain minus the true strain at the necking point, $(\epsilon - \epsilon_n)$. The curves they generated were satisfactory for approximate corrections

but in order to determine the actual correction the actual ratio of d/R must be measured. [Refs. 9: pp. 21-22, 13]

D. TEMPERATURE EFFECTS ON MATERIAL BEHAVIOR

Strength and plastic deformation are temperature dependent phenomenon with the controlling mechanisms existing at the crystallographic scale. Resistance to plastic deformation is determined by the shear stress required to make dislocations glide or move in their slip planes. There are temperature and strain rate dependent components of this stress. The stress applied is required to enable the dislocation to overcome barriers to movement such as precipitates, grain boundaries, and other dislocations. These examples are considered long range fields. Another basic type of barrier to movement in any crystal lattice is a short range barrier called a Peierls-Nabarro barrier. This barrier results from the inherent resistance of the crystal lattice to movement of dislocations. [Ref. 10: 320-326]

A dislocation is a defect in a crystal lattice which arises from the addition or omission of a planar series of atoms. Movement of a dislocation comes about from a movement of atoms in the lattice. The Peierls-Nabarro barrier can be thought of in a simplistic manner as the resistance offered by neighboring atoms to the movement of the atom in an ordered structure. The energy required to overcome this barrier is called the Peierls-Nabarro energy. At temperatures near room temperature (20°C) this energy is predicted to be relatively low but at low temperatures, in materials with strong directional bonding including iron, these stresses increase exponentially as absolute zero (0°K) is approached and are responsible for a significant portion of the yield strength of the material. [Ref. 10: pp. 324]

III. EXPERIMENTAL PROCEDURE

A. MATERIAL AND SAMPLE PREPARATION

A section of 1-1/4 inch (32 mm) HSLA-100 plate (Plate # 5644-16B) from the trial commercial heat of HSLA-100 was provided by the David Taylor Naval Ship Research and Development Center for use in this research. The plate was heat treated by the supplier by solution treating at 949°C (1650°F) for 70 minutes and water quenching and then aging at 566°C (1050°F) for 70 minutes and water quenching. The strength properties listed by the supplier are listed in Table 2.

TABLE 2
STRENGTH PROPERTIES OF HSLA-100 PLATE # 5644-16B
(AS REPORTED BY THE SUPPLIER)

	Yield Strength (ksi)	Ultimate Tensile Strength (ksi)	Percent Elongation	Percent Reduction in Area
Top Transverse	101	147	22	65
Bottom Transverse	106	139	23	65

Reference 14 noted the material properties observed in his research deviated significantly from those listed in Table 2 with much higher yield and tensile strengths. This was confirmed separately by David Taylor NSRDC and through subsequent testing of various additional heat treatments a determination was made to additionally heat treat this steel at 621°C (1150°F) to bring the yield strength within the desired range of 100 to 120 ksi (689 to 758 MPa).

Tensile blanks, measuring approximately 5/8 inch square by 4-1/2 inch long, were cut from the plate transverse to the rolling direction. Three tensile blanks were wired together with spacers and an additional blank for internal temperature monitoring. The set of tensile blanks was then placed in a furnace stabilized at 621°C (1150°F) and aged at 621°C ± 1 percent for 60 minutes and water quenched. The oxides that formed on the surface of the bar during the aging process were removed from the face of the bar perpendicular to the rolling direction, and the hardness was determined on the Rockwell C scale by the average of 5 measurements. The average of all 52 blanks aged was RC 24.8 with a standard deviation of 0.98, corresponding to the accuracy of the testing apparatus used. This average hardness converts to an approximate tensile strength of 118 to 122 ksi (814 to 841 MPa). The resultant microstructures are shown in Figures 4 and 5.

In the light micrograph of Figure 4, the microstructure is seen as a fine banite with banding lightly evident from this aspect, looking at the side of the plate, an end view of the samples. Figure 5 is a TEM micrograph illustrating high dislocation density and copper precipitates evident within grains and at the grain boundaries, visible as oblong spots.

On completion of the aging two blanks were machined into uniform gage length samples in accordance with Figure 6 (a) and the remainder of the tensile blanks were machined into hourglass shaped specimens in accordance with Figure 6 (b). The diameters of the finished tensile specimens were then measured and recorded.

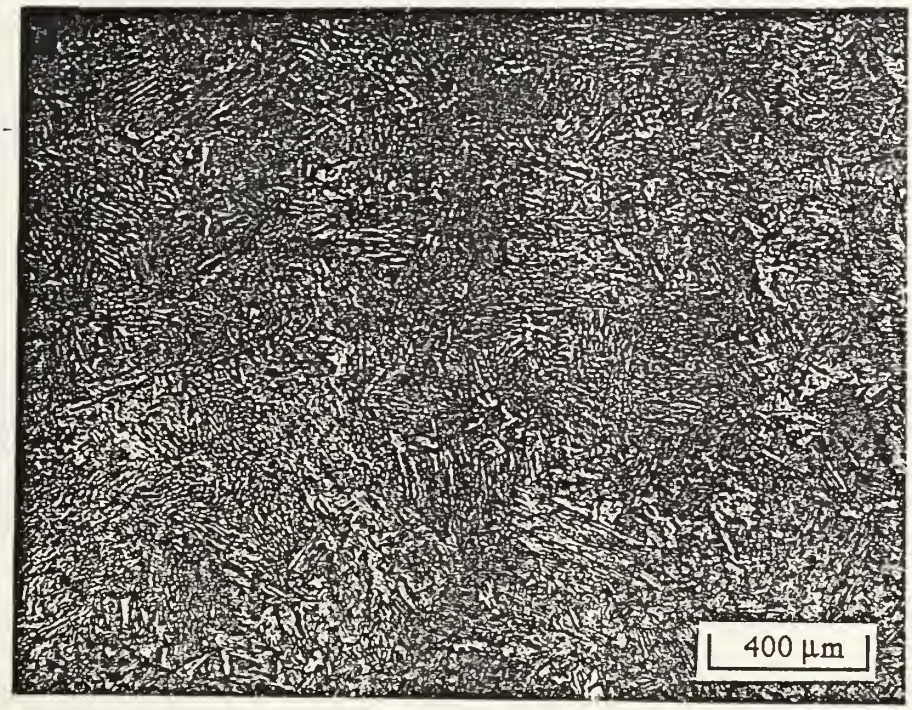

Figure 4
Light Micrograph of Aged HSLA-100 • 2 percent Nital Etch for 25 seconds
500X

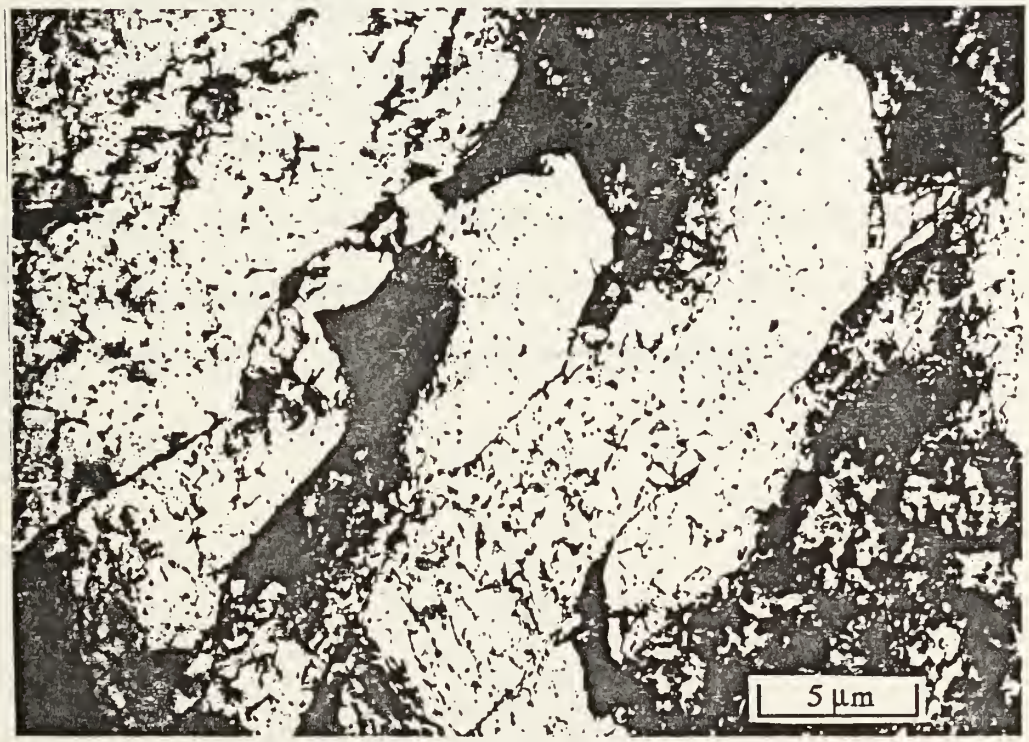

Figure 5
TEM Micrograph of Aged HSLA-100

B. TEST APPARATUS

Tensile tests were conducted with a MTS 810 Material Test System including as the major functional parts (all manufactured by MTS): 409 temperature controller, 464 data display, 410 digital function generator, 445 controller, 413 master control panel, Thermotron environmental control chamber, 10 ton load cell, 632.19B diametral extensometer, and load frame with hydraulic actuators. The diametral extensometer was required to follow the deformation in the neck to failure using the modified, smaller radius, tips described in Reference 14.

Several modifications to the basic to the basic setup were made to improve temperature control. Phenolic washers were used in all unions in the actuator train to restrict heat flow into the system. For cooling to the sample grips, the liquid nitrogen tubing was split so that both grips would receive equal flow of nitrogen and the tubing size was increased to 3/8 inch from 1/4 inch to allow the nitrogen gas which boiled off to escape easier. Without the larger tubing the backpressure created by the nitrogen boiling off could shut off the flow of nitrogen to the grips. These modifications resulted in slower temperature changes and allowed faster response to the changes, thus better temperature control. With this setup alone temperatures to -180°C (-308°F) were easily attained and controlled. Photographs of the MTS control system, grips and chamber are shown in Figure 7 (a) and (b).

NOTES: 1. All dimensions in inches.
2. Tolerances as per ASTM tensile specimen standards.
3. Specimen gage length to be perpendicular to plate as rolled direction.
4. Gage length shall be 32 rms.
5. Mark with applicable specimen number on both ends.

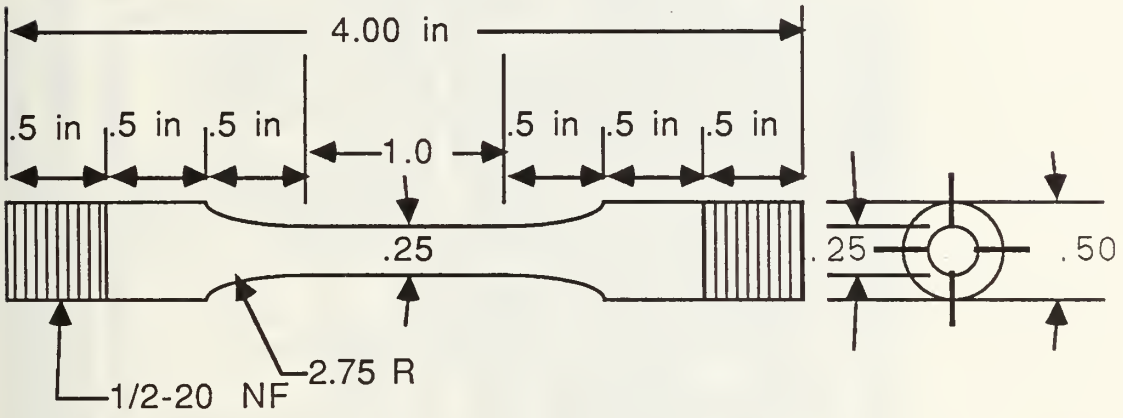

(a.)

NOTES: 1. All dimensions in inches.
2. Tolerances: As per ASTM tensile specimen standards.
3. Specimen gage length to be perpendicular to plate as rolled direction.
4. Reduced section area of specimen shall be polished in a manner parallel to specimen longitudinal axis to 32 rms.
5. Mark with applicable specimen number on both ends, vibrating type engraving tool is permissible.

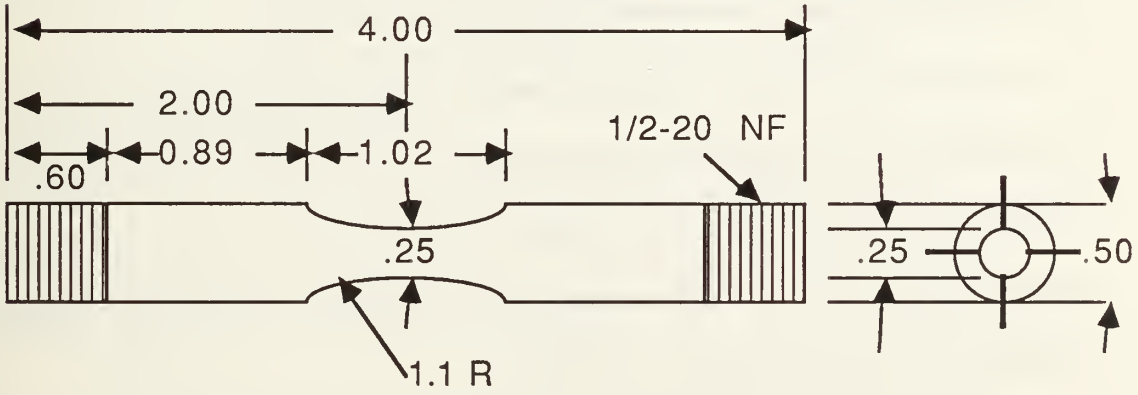

(b.)

Figure 6
Tensile Specimen Drawings

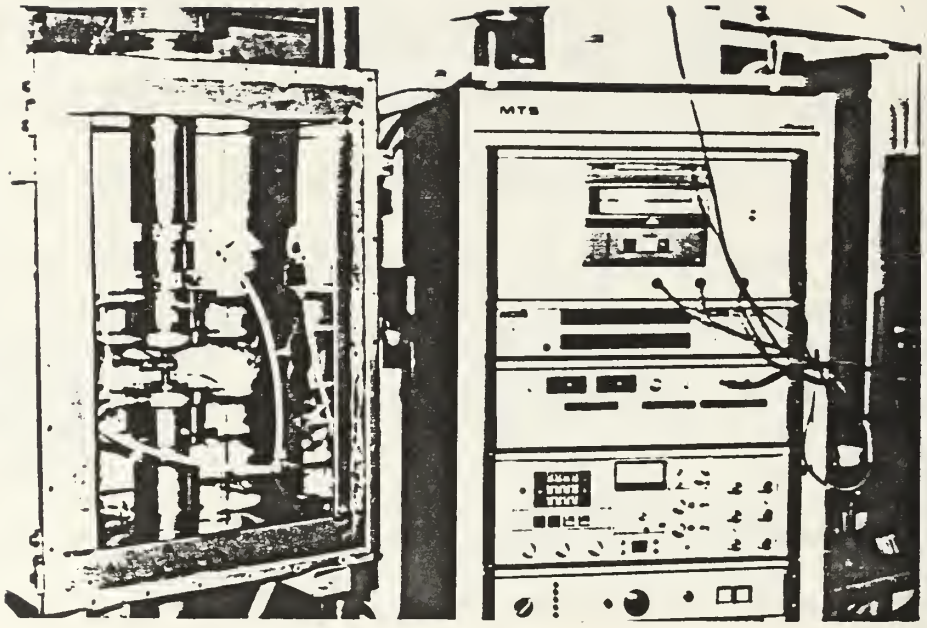

Figure 7
MTS Function Generator, Controls and Test Assembly

Temperature control was achieved by two different methods dependent on the temperature desired. At temperatures below -150°C (-238°F) the cooling circuit switch had to be manually cycled and at temperatures above that the installed temperature controller was capable of maintaining the temperature within ±2°C. The top grip temperature was monitored internally and was the sensing point for the controller. Temperature was sensed by five chromel-alumel thermocouples sensing chamber air temperature, top and bottom grip temperature, and sample temperature above and below the hourglass gage length. The thermocouples were calibrated in liquid nitrogen indicating -189°C for an actual temperature of -195.8°C.

Procedures for use of the tensile test system and general conduct of testing are those provided by MTS for this system modified for the specific requirements of these tests by Hamilton in Reference 14. An additional check sheet was used to emphasize particular parts of the testing process.

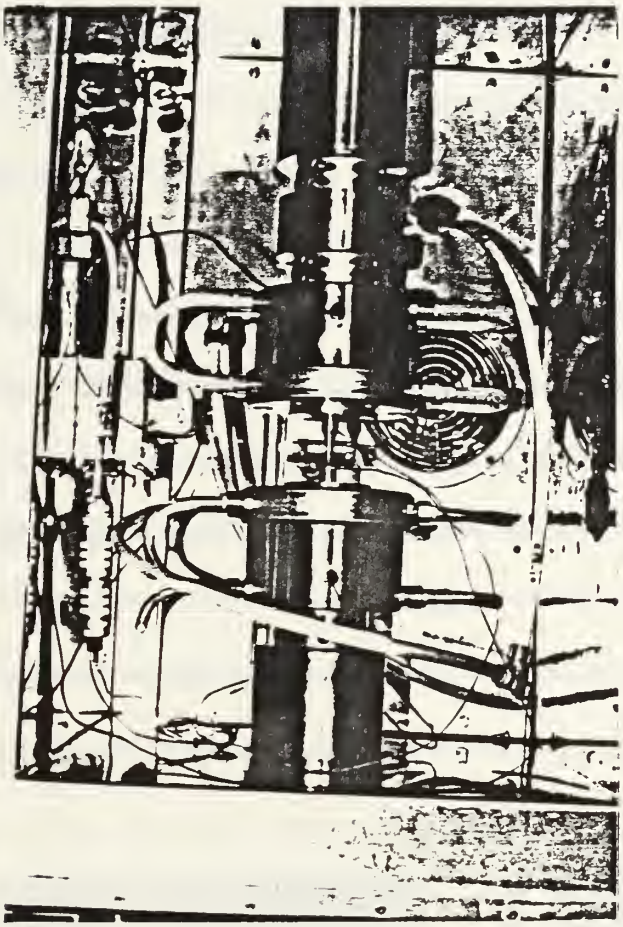

Figure 8
Environmental Test Chamber, Actuator, and Grips

C. DATA COLLECTION AND REDUCTION

During testing, progress of the test was monitored and recorded using an X-Y plotter sensing the displacement and load voltages. This plot was an important indication of experimental irregularities and was used to verify information gathered by other means. The load and displacement voltages were sensed, converted, and recorded using a Hewlett-Packard 3437A system voltmeter, and 3497 data acquisition/control unit, both controlled by a Hewlett-Packard 9826 computer all shown in Figure 9. Software for the data acquisition process was a truncated form of 'JHCOLLECT" written by Hamilton and provided in Reference 14. Modifications to the program included sampling only load and

displacement voltages, increasing the size of the arrays for data storage, and sampling at a constant frequency throughout the test. The increased size of arrays was required to store large amounts of data collected at intervals of less than a second. The uniform sampling provided that no one portion of the curve would be weighted differently in a least squares reduction routine.

The large data files, containing approximately 1800 to 2200 data sets, were stored on disc in the Hewlett-Packard computer then retrieved at some linear interval to select approximately 110 load/displacement data points from the start of the test until failure. These data points were then manually transferred into a Macintosh personal computer for analysis and plotting of the resultant curves.

Fracture surfaces were examined by scanning electron and light microscopy for examination of failure types. Metallographic examination was also conducted by light microscopy.

Figure 9
Data Acquisition System

IV. ANALYSIS AND RESULTS

A. DETERMINATION OF THE ELASTIC MODULUS

In order to convert true strain to true plastic strain, the elastic modulus for the material was first determined. The sole purpose for the uniform gage length samples was to achieve this end. The Young's modulus for the re-aged HSLA-100 in the transverse direction was determined using the two uniform gage length samples machined from the plate in the transverse orientation, longitudinal extensometer and the experimental setup as described previously. Each of the two samples were loaded slowly to what was expected to be about 60 percent of the yield strength, 3.2 kips. The voltages were recorded on the X-Y plotter, data converted to stress/strain and the slope for each of the two samples, $d\sigma/d\epsilon$, determined. For the two samples, specimen numbers 16 and 17, the elastic modulus were found to be 24, 053 ksi and 23, 953 ksi respectively for an average Young's modulus of

$$E = 24{,}000 \text{ ksi } (1654.7 \text{ MPa}).$$

This value is close to that reported by Hamilton for the as received HSLA-100 (24,140 ksi)[Ref. 14].

Because of the expanded scale of the plot required for the determination of the the elastic modulus improved chamber supports were manufactured to remove a small discontinuity in the plot at very low loads and strains.

B. INITIAL TESTING AND ANALYSIS OF HOURGLASS SPECIMENS

Four samples, numbers 39 to 42, were initially tested to the practical full travel of the diametral extensometer, about .077 inches (0.736 in/in true strain), in strain control

then manually broken in stroke control. The computer data acquisition only collected the initial full range travel of the extensometer. The final radius of curvature of the neck and final diameter were measured and recorded. The data, converted to the form of load and displacement, was stored and a reduced number of data points transferred for analysis.

1. Computer Aided Determination of the Voce Coefficients

To determine the coefficients for this equation is difficult since three unknowns are involved. However using one of the derivative forms of the Voce equation results in an easier solution. Voce noted a linear relationship when he plotted the true strain versus the quantity $Ln[(S_\infty-S)/(S_\infty-So)]$. The characteristic strain, A, would be the slope of this line. Since the intercept, $Ln(S_\infty-So)$, is a constant, a plot of the equation: $\epsilon=-A\ Ln[S_\infty - S]$ should yield a straight line, but this equation still has two unknowns. [Ref. 11: p. 161]

The recommended solution of this problem in is to select a true stress higher than any observed, set it equal to S_∞, and iterate this value of S_∞ until the straightest line value for S_∞ is found using a comparative method such as the correlation coefficient [Ref. 11: pp. 166-169]. A computer program in Microsoft BASIC was written to do this. Several versions for the program were written for calculation of the Voce coefficients for true stress/true strain, Bridgman corrected true stress/true plastic strain and so on but only the true stress/true strain version is included as Appendix B.

Figure 10 shows the effect of changing S_∞ on the slope (-A) of this relationship. As the true stress approaches S_∞, the difference between S_∞ and the true stress, S, becomes smaller. The Ln function becomes more sensitive to fluctuations in the load resulting in the spikes in this plot which are amplified at higher stresses. The gap in the data points results from stopping and restarting the test. The values for the constants derived by this method are very sensitive to the data from each extreme (high and low stress) of the plot. The data

below the yield point approaches the horizontal so inclusion of these points in a least squares fit will pull the straight line fit to the right at the bottom, lowering the value of the characteristic strain and also produce a lower value of S∞ and So for the best least squares fit. From the actual data set of Figure 10, (sample 50) the final value of S∞ was determined to be 265.0807 ksi, a characteristic strain of 0.7891093; the correlation coefficient for the equation using these values for the contants is 0.9968 (a correlation coefficient of 1.0 indicates a perfect linear fit).

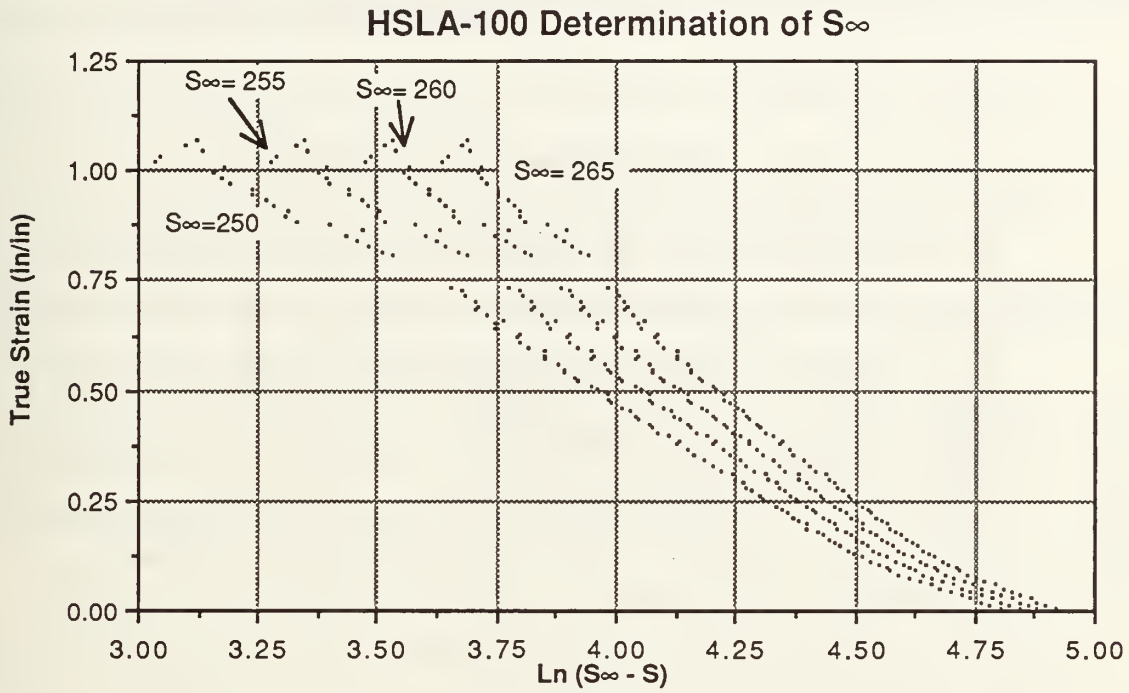

Figure 10
Determination of S∞ and the Characteristic Strain

Analyzing the data of these first four tests (samples 39 to 42) brought about several important results. The first problem was that of determining the actual load/displacement at failure. To determine this point the final diameter was measured from the failed sample and the load was estimated from the X-Y plot. The results of sample number 39 are typical of the results and the plot of true stress/true strain is shown in Figure 11. The larger

points correspond to the first point considered in the Voce analysis (approximately the yield point), the point of maximum load and the last data point acquired. The point on the top right is the estimated failure point; clearly this point is not correct because an extrapolation of the stress-strain data from the last data collected would not even come close to this point. In addition the value for S_∞, where the true stress should reach a final asymptotic value, was calculated as 226.4978 ksi, far below the maximum true stress estimated from the fracture point. This was also determined to be low because the lack of data in the high stress region biases the linear regression to the low stress region resulting in low values of A and S_∞.

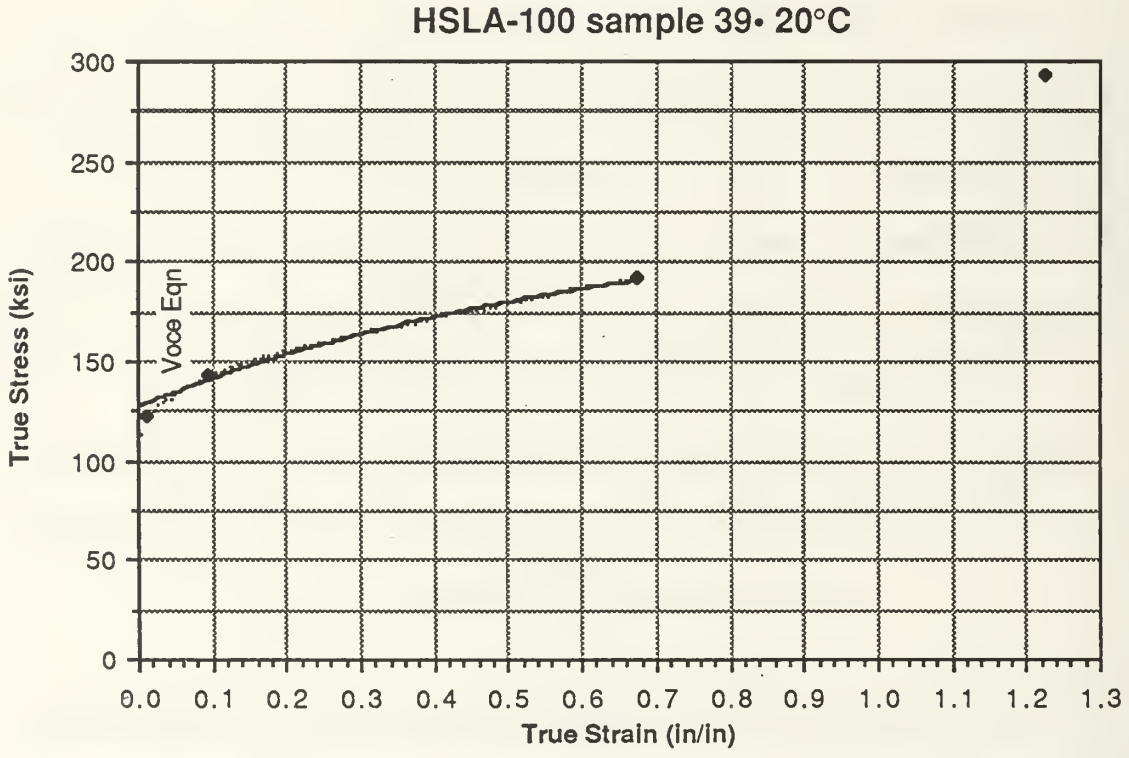

Figure 11
Estimate of the Voce Equation and Failure point - Sample Number 36

2. Modifications to the Testing Procedure

Based on these results it was determined that it was necessary to collect strain data right up to fracture. This would extend the curve, giving a better indication of the actual stress at failure and properly weight the least squares curve fit to find S_∞.

Another series of measurements and analyses being conducted at the same time dealt with the Bridgman correction, the measurement of the radius of curvature and how it changes with the strain. Reference 9 [p. 21] indicated the change in the Bridgman correction could be roughly correlated with the difference between the instantaneous true strain and the strain at the necking point (maximum load) and that this could be used for determining approximate Bridgman corrections as a function of strain. To confirm this, one test was conducted where the loading was interrupted at several points between the maximum load and failure. The radius of curvature and diameter would be measured at each interruption. For future tests it was also decided to use the full range travel of the extensometer (0.077 inches) as a stop point for measurement of the radius of curvature giving another indication of the trend of the Bridgman correction.

To accomplish testing in this manner a thin (about 0.040 inch) piece of copper was shaped to fit snugly on one of the extensometer tips. This additional 0.040 inch would be sufficient to extend the range of displacement of the extensometer to accommodate the largest deformations experienced to that time. To correct for the measured displacement change that occurred when the copper foil was inserted, this displacement (about .040 inches) was added to all of the data collected during the retrieval and transfer of the data files.

C. COMPLETION OF TESTING HOURGLASS SPECIMENS

A total of 22 additional hourglass shaped specimens were tested at temperatures varying

from -189°C to 37°C (-308.2°F to 98.6°F) with no appreciable difficulties encountered. Temperature was maintained at ±5°C at temperatures from -150°C to -180°C and at than ±2°C otherwise and the strain rate was constant at about $1x10^{-3}$ in/in sec.

1. Voce Coefficients and Comparison to the Hollomon Power Equation

The Voce equation coefficients were determined for 21 tests using the computer program described in Appendix B. A typical plot of the load/displacement is shown in Figure 12 (a.). The most notable feature of this plot is the manner in which the material fails. A sudden drop in load (at a displacement of 0.1 inches) occurred just before the final fracture. This phenomenon was noted in some form at all temperatures greater than -100°C. The true stress/true strain plots of these data and logarithmic plots are shown as Figure 12 (b.) and (c.). The rapid dropoff of the load is also seen in these plots. Another feature of the logarithmic plot, which is slightly visible, is a small discontinuity, or small change in slope at about the maximum load point. Since data prior to the yield point and in the last region of the rapid drop in load cannot be described by the Voce equation they were not considered in the Voce analysis. The load/displacement or stress/strain plot had to be viewed first to determine the region which could be described by the Voce Equation. The regions not included in the analysis are relatively small at either end of the curves and more information can be gained by their exclusion.

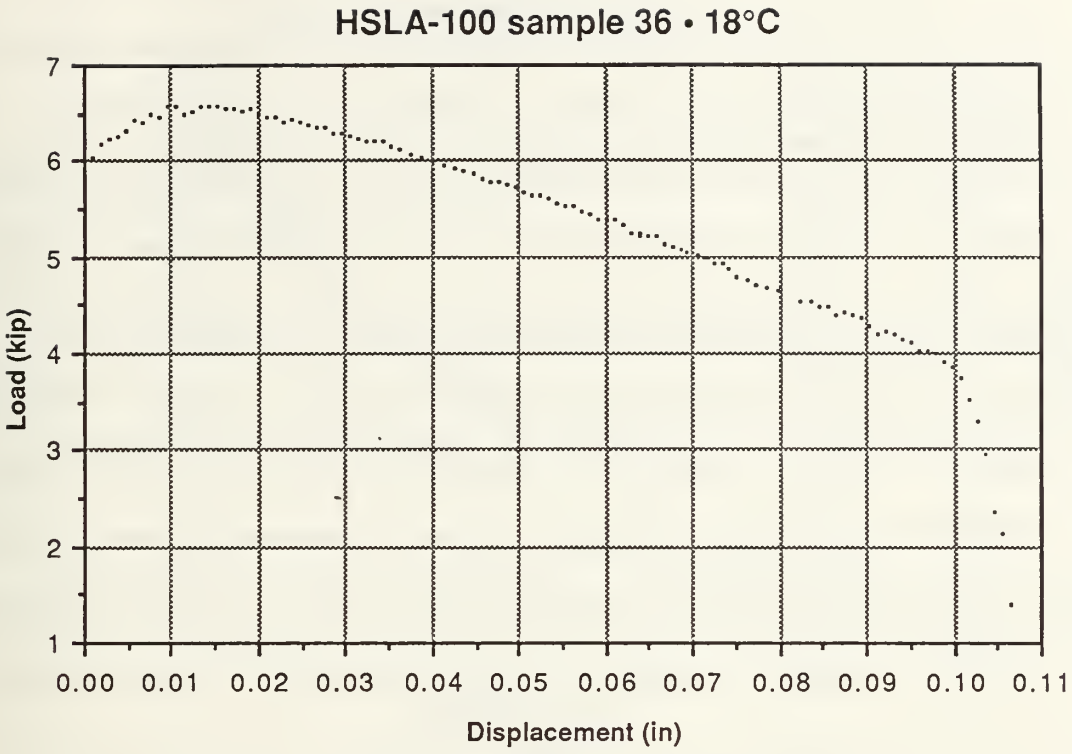

(a.)

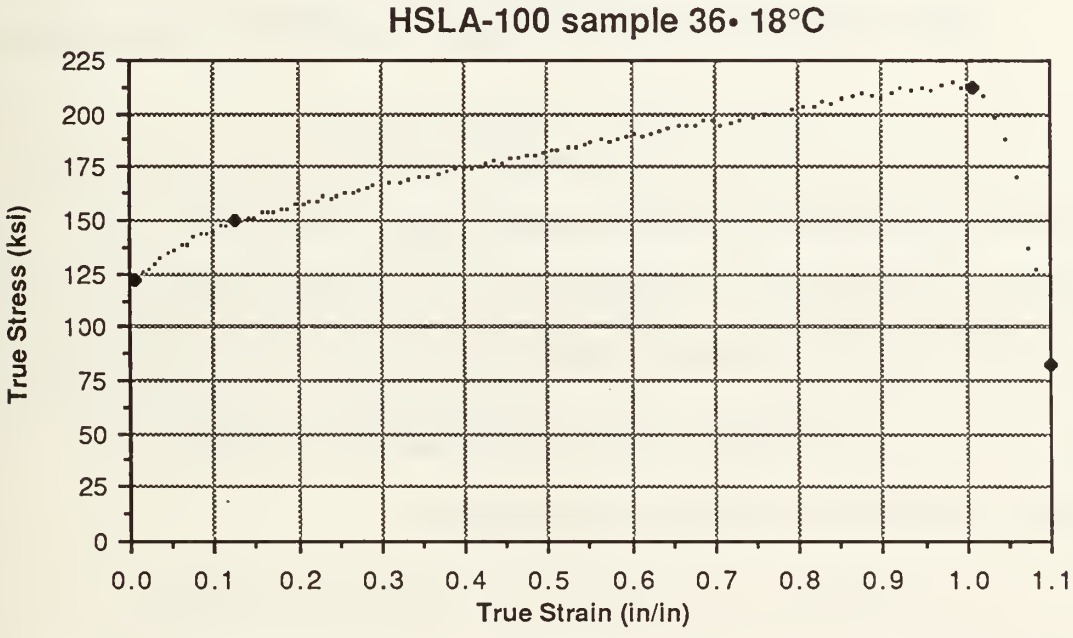

(b.)

Figure 12
Typical Experimental Load/Displacement and True Stress/True Strain Plots

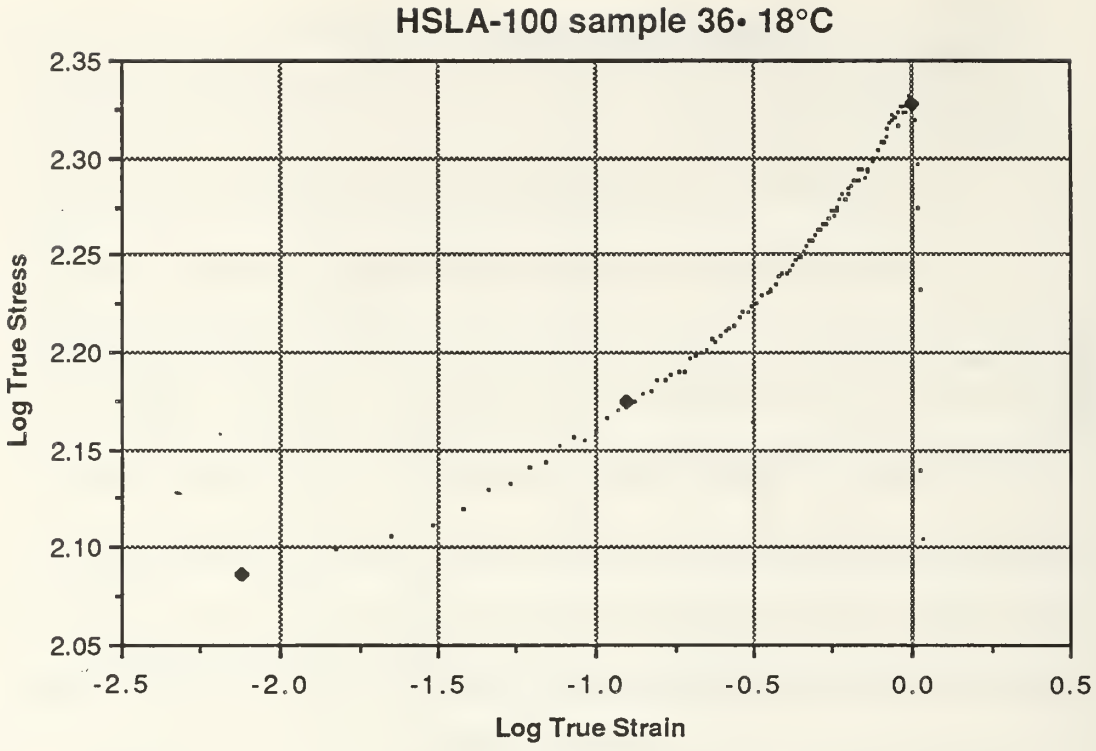

(c.)

Figure 12
Typical Experimental Load/Displacement and True Stress/True Strain Plots

If the Hollomon power equation is appropriate, the log true stress versus log true strain should be a straight line. When a plot similar to Figure 12 (c.) is viewed on an expanded scale of log true stress ranging from zero to 2.3 on the Y-axis the resultant plot does appear to be quite linear, however by examining the plot on the magnified scale as shown in Figure 12 (c) it is apparent that a straight line will not describe the curve accurately. The Hollomon power equation has the form:

$$\sigma = K \epsilon^m \qquad \text{or:} \qquad \log \sigma = \log K + m \log \epsilon$$

where K is the strength coefficient and m is the strain hardening exponent. By simply doing a least squares fit of log σ as a function of log ϵ, m is the slope of the line and the intercept

is logK.

Using this method for the solution of the Hollomon power equation coefficients and the method previously described for the solution of the Voce coefficients, for all of the tests, the results are as listed in Table 3.

For all data sets, the Hollomon power equation fit the data with correlations ranging from .9492 to .9836 and the Voce equation fit with correlations of from .9937 to .9993 for the same regions of the curves. From the point of correlation alone the Voce equation would appear to fit the data much better. Looking at a typical plot of the true stress/true strain data with the predicted curves overlayed as shown in Figure 13, the Voce equation does fit the data much better. Neither of these equations fit well in the region of low strains so for comparative purposes the fifth data point is arbitrarily chosen as the first point compared and the last point used in the curve fit is the last considered. Starting from this premise, the percentage error of the predicted curve is calculated by the equation:

$$\text{Percent Error} = [\text{ABS}[\sigma - \sigma_c]/\sigma] * 100$$

For the Hollomon power equation the maximum single point error is 8.30 percent and the maximum average error for any single curve is 3.80 percent. The fit appears to be worse at low temperatures and gets better at intermediate temperatures (-117°C). The best average error for the Hollomon power equation is 1.58 percent at -117°C.

TABLE 3

VOCE AND HOLLOMON EQUATION COEFFICIENTS

Temp (°C)	sample number	Voce S_∞ (ksi)	Voce So (ksi)	Voce A (in/in)	Hollomon K (ksi)	Hollomon m
-189	46	491.0986	175.2839	1.360575	300.9788	.1523583
-176	28	399.506	165.2733	1.095739	285.465	.1692908
-170	52	389.2834	169.0419	1.100783	281.1485	.1604666
-154	34	356.417	157.7226	1.077566	262.1936	.1601815
-150	47	380.1898	156.2891	1.176447	262.168	.157335
-140	26	385.2167	154.5706	1.309195	261.0666	.1674174
-133	25	298.439	148.9738	.7496496	249.049	.1572877
-132	37	309.1749	144.9128	.8607823	245.0456	.1610462
-124	24	337.1254	156.5421	1.194708	244.7035	.1436531
-117	19	257.3777	143.9943	.5703971	232.392	.143561
-110	49	282.4977	145.829	.8121898	232.2654	.1440436
-101	23	309.5079	145.3076	.9910815	236.4248	.1517314
-91	22	253.6235	140.7949	.655102	223.2169	.1433506
-80	50	265.0807	138.1622	.781093	220.8118	.1458434
-71	20	308.4355	140.5525	1.072554	230.6979	.1585906
-56	31	293.8192	137.9099	1.065468	222.25	.1528224
-30	51	279.0695	132.6547	1.01008	214.241	.15167
0	30	271.9845	133.1512	.9848082	211.7802	.1474638
18	36	258.9012	131.1185	.9638342	203.3129	.1383482
18	35	272.7748	129.2532	1.144794	202.0873	.1440793
37	27	245.5962	125.0026	.8919725	197.183	.1418691

The Voce equation on the other hand has a worst single point error for all of the data sets of 4.55 percent and a worst average error of 1.21 percent. The best average error was 0.43 percent at -150°C. The maximum errors and average error are less for the Voce equation for all data sets. Sample number 50, shown in Figure 13, has the smallest difference between average errors of the Hollomon power equation and Voce equation for the tests conducted. Based on these results the Voce equation was determined to fit the data better, and the Hollomon equation was not considered for further investigation.

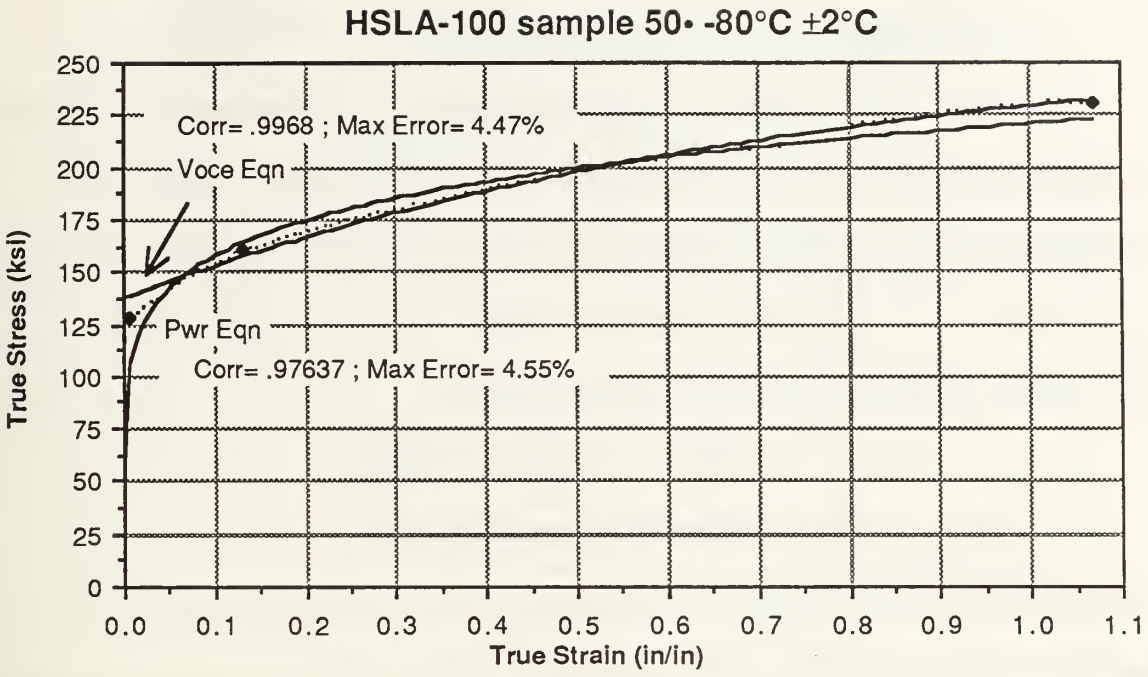

(a.)

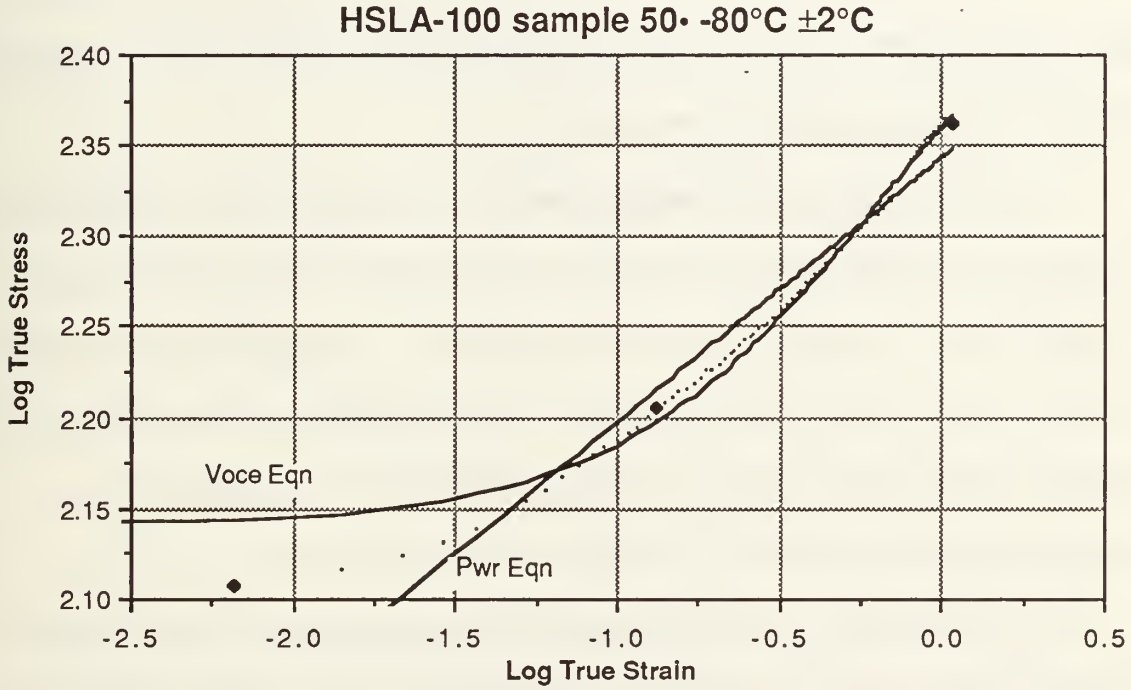

(b.)

Figure 13
Comparison of the Voce and Power Equations

2. The Voce Equation as a Function of Temperature

Several forms of equations were considered for a fit of the Voce stress coefficients as a function of temperature including exponential and logarithmic forms. The final form decided upon was an exponentially decaying function typically used to describe a thermally activated event such as overcoming the Peierls-Nabarro stresses. The Voce stress coefficients as a function of temperature are found to be:

$$S\infty(T) = Co + [C1*\exp(Tc/T(°K))]$$

$$So(T) = Co + [C1*\exp(Tc/T(°K))]$$

where Co and C1 are constants with units of stress, Tc is a constant with units of temperature in degrees Kelvin, and T(°K) is the temperature of the test in degrees Kelvin. As the test temperature becomes very large compared to Tc, the exponential becomes approximately equal to 1 and the sum of Co and C1 then becomes the value of stress which is asymptotically approached at high temperatures.

The method for solving this equation was similar to that of the Voce equation except in this case the stress coefficient is the dependent variable and the quantity exp(Tc/T) is the independent term. The value of Tc was incremented from 1 to 300°K and the most linear value of Tc was the one from which the slope, C1, and the intercept, Co, were calculated. The linearity was again measured by the correlation coefficient. The plot of the stress coefficient data points and the curve fit to them is shown in Figure 14.

The characteristic strain, A, plotted against temperature yielded a random scatter of data points with no apparent correlation as shown in Figure 15. The average for all of the A values was found to be 0.99375 and the median was 1.01008 so the mean was arbitrarily chosen to be the value of A across all temperatures (A(T)= constant= .99375).

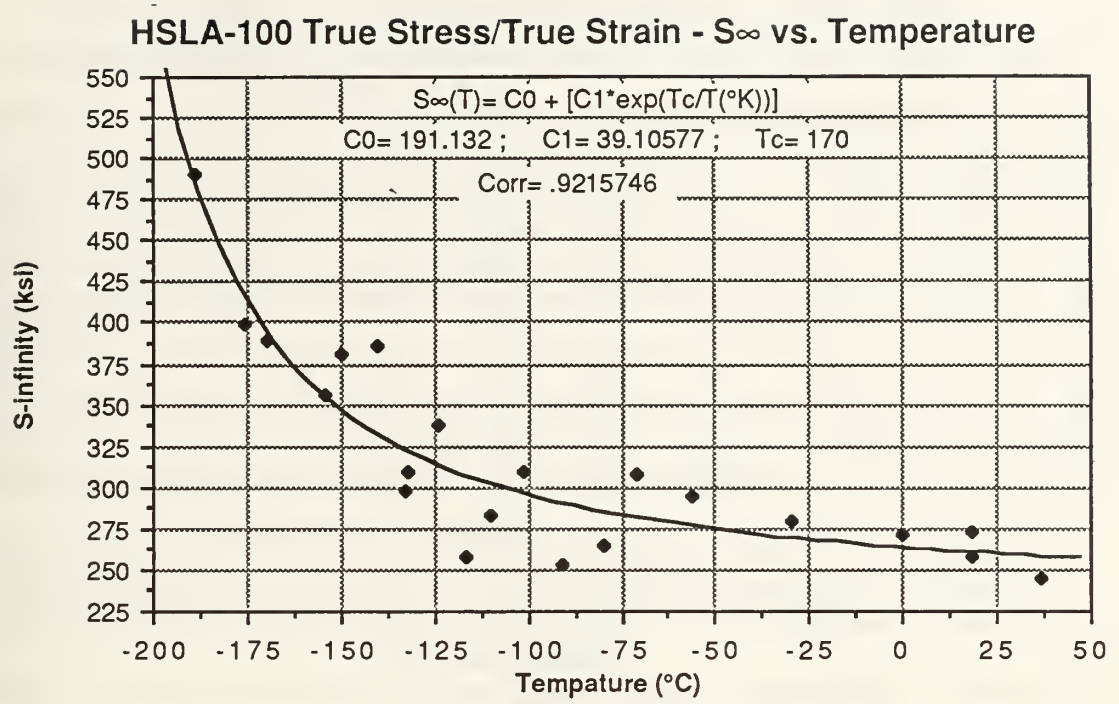

(a.)

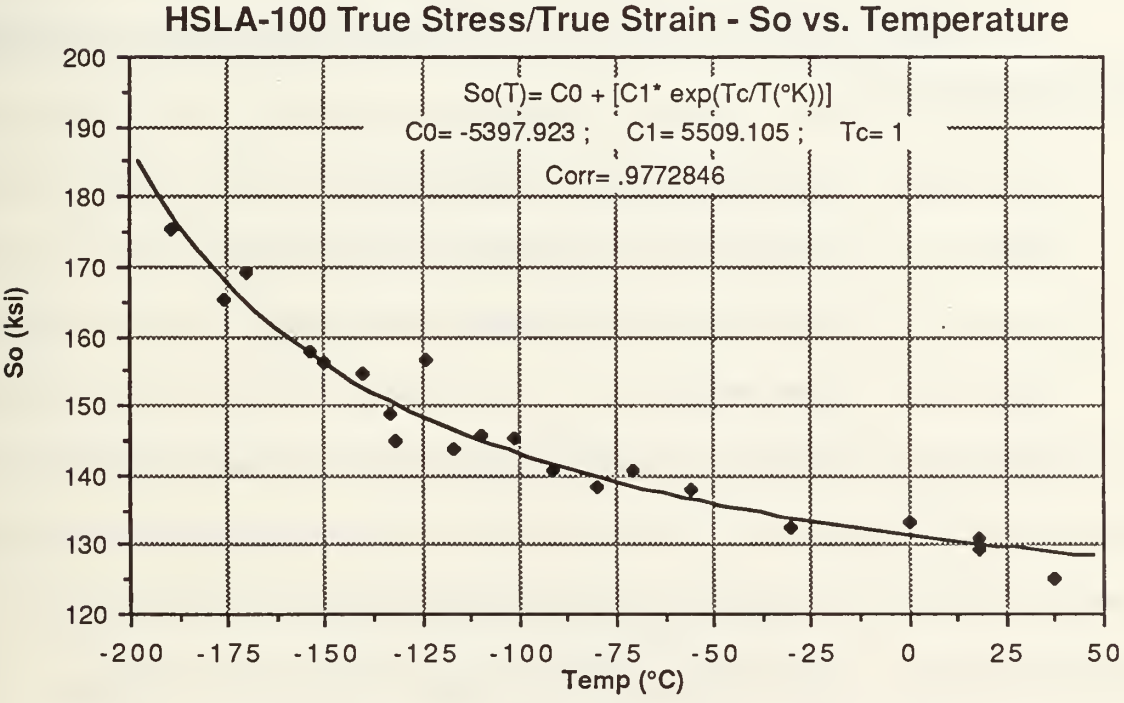

(b.)

Figure 14
Voce Stress Coefficients as a Function of Temperature (1)

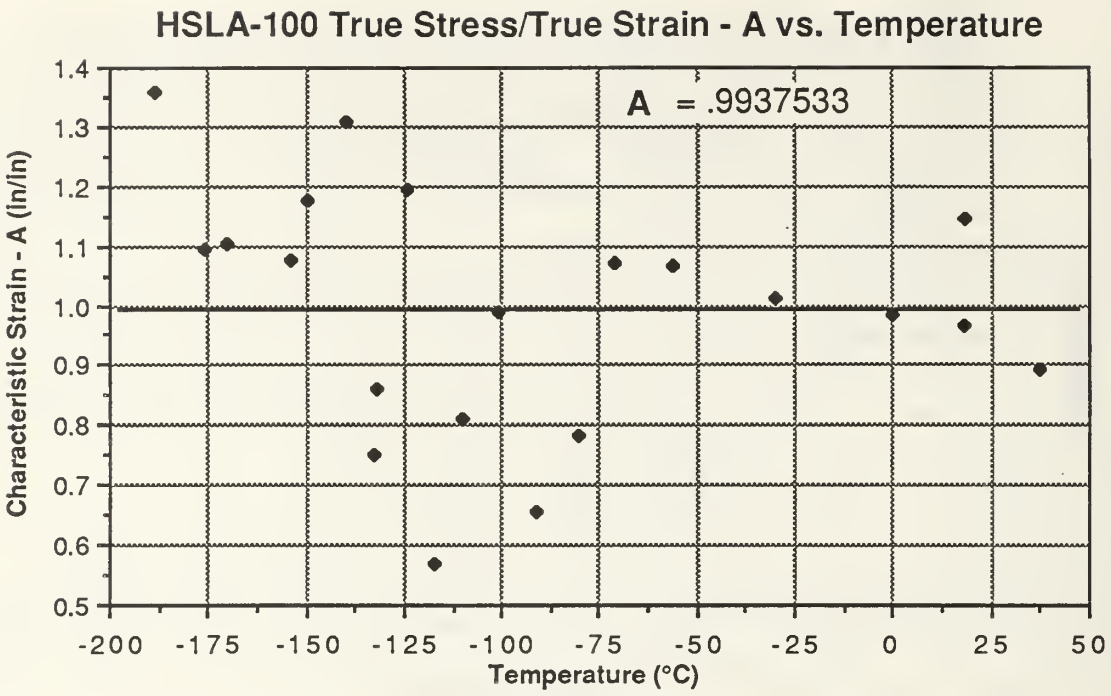

Figure 15
Characteristic Strain as a Function of Temperature

By combining the individual equations, the Voce equation as a function of temperature and strain was derived.

$$S = S_\infty(T) - \{[S_\infty(T) - So(T)]^*\exp(-\epsilon/A)\}$$

where $S_\infty(T) = 191.132 + [39.10577^*\exp(170/T(°K))]$

$So(T) = -5397.923 + [5509.105^*\exp(1/T(°K))]$

and $A = .9937533$

A test expected to have a good fit and another test expected to have a poor fit based on the differences between the actual S_∞ and So and that predicted by the above equations were selected to examine the accuracy of the overall predictions based on these temperature dependent equations. The fit of the predicted curve for sample 46, which had actual coefficients right on the predicted curves, and sample number 26, which has S_∞ predicted about 50 ksi lower than the test indicated, are shown in Figure 16. For orientation the label, Voce(T), is the curve fit as a function of ϵ and T, the other is the Voce equation curve

fit for that individual test. The characteristic strain and the S_∞ have some sort of balancing relationship. That is, even though a difference may exist between the predicted values of S_∞ and A with respect to the value of the constants determined from the individual test, the overall stress-strain prediction may be excellent. This will not always be the case, however.

The next step in the analysis was to assume that the characteristic strain, A, is a constant as already assumed and recalculate the stress coefficients. Since the mean and median bracket the value of 1.0, A is assumed constant and equal to 1.0. With this assumption the values for S_∞ and So are recalculated with a simple slope and intercept calculation; stress the dependent variable, strain the independent variable, S_∞ equal to the intercept and the slope equal to $-(S_\infty - So)$. The correlation coefficient for all version 2 individual curve fits were greater than .990. The results were then plotted and an exponential curve fit to to the new stress coefficient data points. The results are shown in Figure 17; by the correlation coefficient alone these curves fits the new coefficient data better than those initially. The coefficients for So did not change significantly but the S_∞ coefficients are much closer to the predicted curve, increasing the correlation coefficient by greater than 0.06. In the same manner as before, the Voce coefficients as a function of temperature are substituted into the Voce equation forming an equation for stress as a function of strain and temperature:

$$S = S_\infty(T) - \{[S_\infty(T) - So(T)]^* \exp(-\epsilon / A)\}$$

where $S_\infty(T) = -78.8051 + [292.1489^* \exp(46/T(°K))]$

$So(T) = -5148.559 + [5261.393^* \exp(1/T(°K))]$

and $A = 1.0$

When T(°K) is much greater than Tc, S_∞ approaches 213 ksi and So approaches 113 ksi.

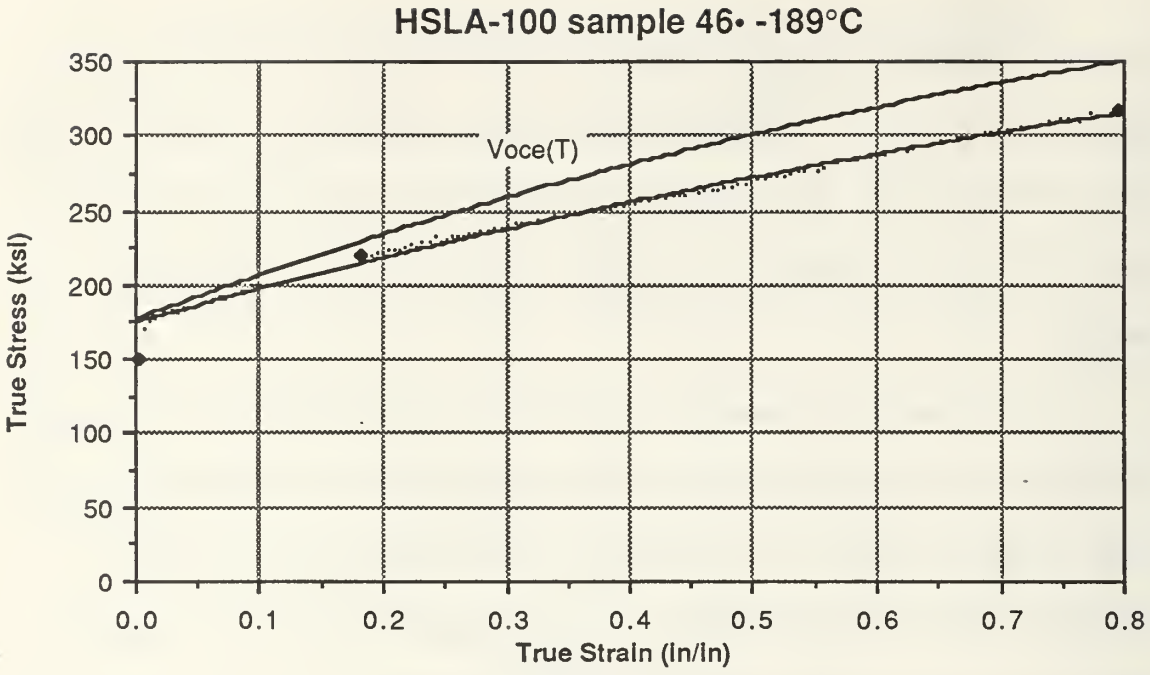

(a.)

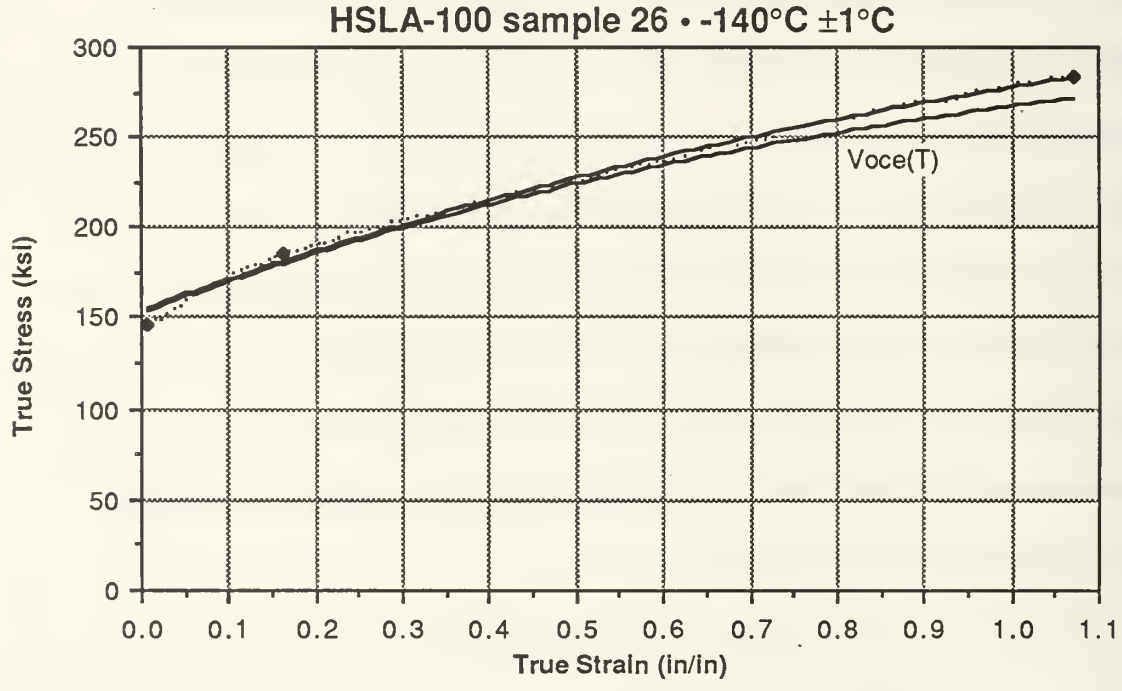

(b.)

Figure 16
Voce(T, ϵ) - Plots of Two Tests

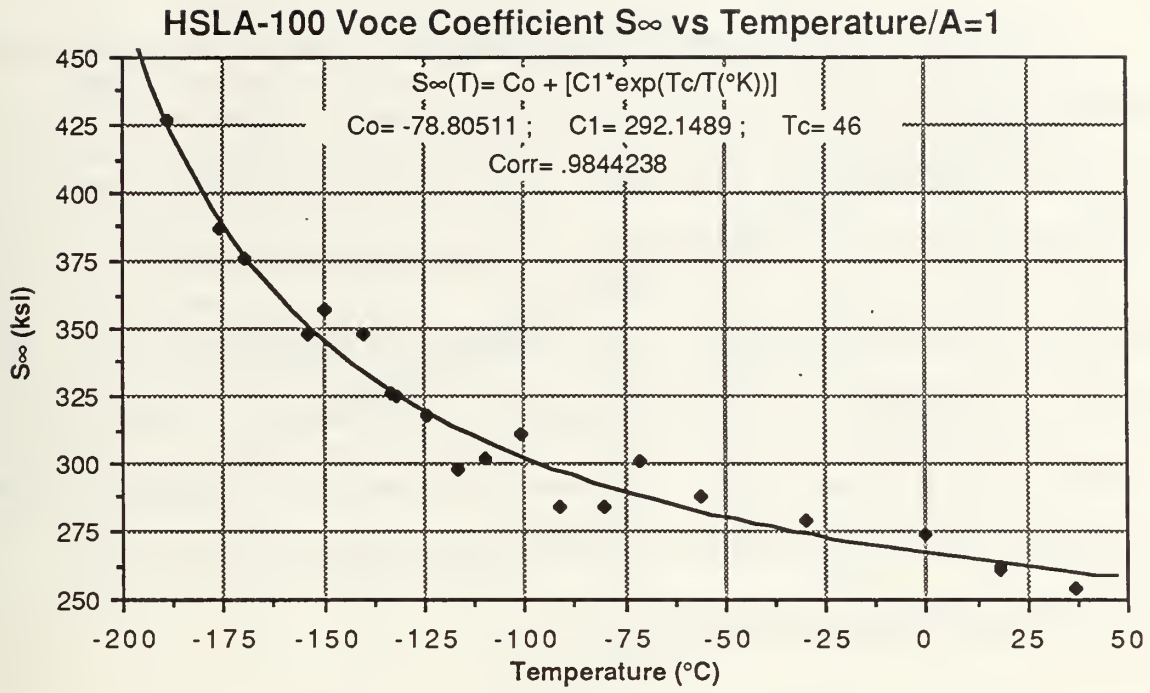

(a.)

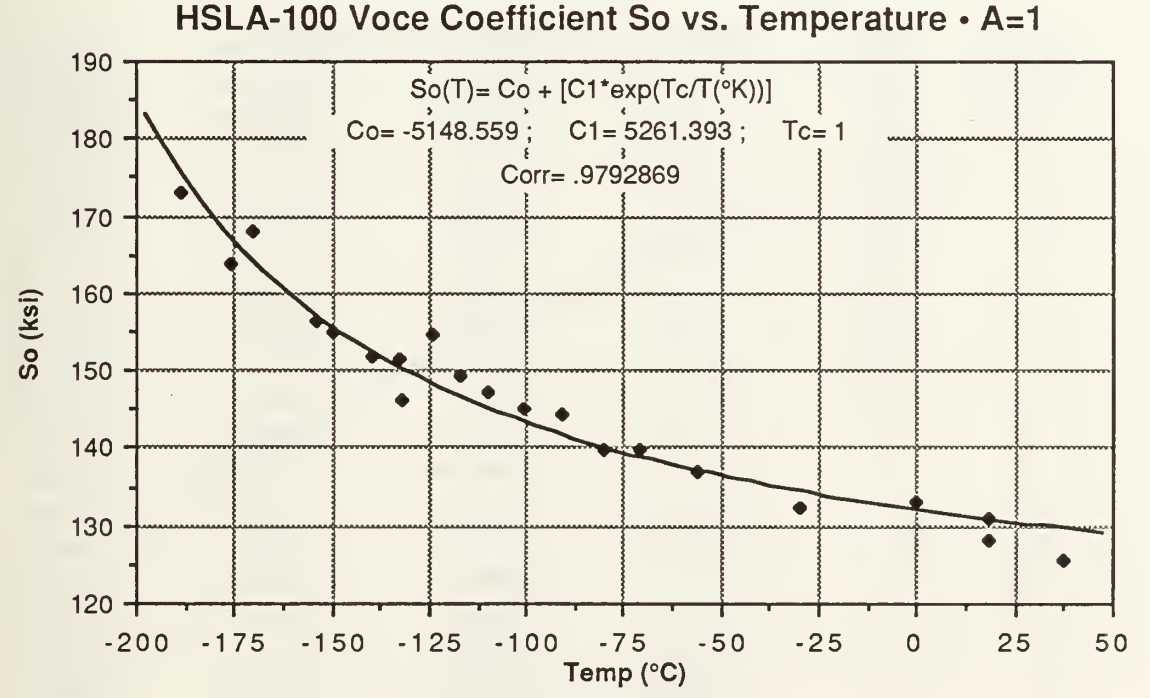

(b.)

Figure 17
Voce Stress Coefficients as a Function of Temperature (2)

Fitting the new Voce equation to the same two curves as before gives apparently more satisfactory results. A comparison of the errors of the two versions is presented in Table 4. The initial coefficients calculated are sometimes better than those calculated for version 2, but overall version 2 is much better. Version 2 shows generally lower single point maximum errors and lower averages. Figure 18 shows the modified version of $\sigma(\epsilon, T)$ using the new coefficients as a function of temperature overlayed with the individual test predictions and data for several tests. The same tests, numbers 26 and 46, are presented as are two other tests, samples 51 and 20, the tests with the smallest and largest average errors, 0.560 and 2.76 percent respectively.

TABLE 4
COMPARISON OF ACCURACY FOR VOCE(ϵ,T) VERSIONS

sample number	Temp (°C)	Max Error Version 1	Avg Error Version 1	Max Error Version 2	Avg Error Version 2
46	-189	11.79377	8.095257	2.179396	.8623438
28	-176	7.796861	5.141882	3.878173	1.28702
52	-170	3.967472	2.03051	2.997622	.9321079
34	-154	3.87577	1.433683	3.495088	1.046242
47	-150	2.674214	1.028046	3.1547	1.370743
26	-140	5.042438	2.307615	4.677677	2.134145
25	-133	3.60902	1.144696	3.60868	.9944419
37	-132	6.272017	.7508031	6.287417	1.196656
24	-124	5.571671	2.8092	5.203831	2.313026
19	-117	4.789085	1.638871	6.210592	2.020577
49	-110	3.813052	1.196474	4.02332	1.452825
23	-101	4.538417	3.012768	3.873194	2.032468
22	-91	3.561259	1.429343	5.00009	1.782425
50	-80	5.269707	1.066175	5.666542	1.546789
20	-71	5.652589	3.804017	4.19193	2.764634
31	-56	3.811433	2.316394	2.7988	1.337599
51	-30	2.569845	1.258869	2.944652	.5596738
30	0	3.998918	2.392466	3.413519	1.762665
36	18	2.750092	.8317102	2.195829	.7063553
35	18	2.871258	.8925604	3.431084	1.259844
27	37	5.589019	1.994318	6.239485	2.401873

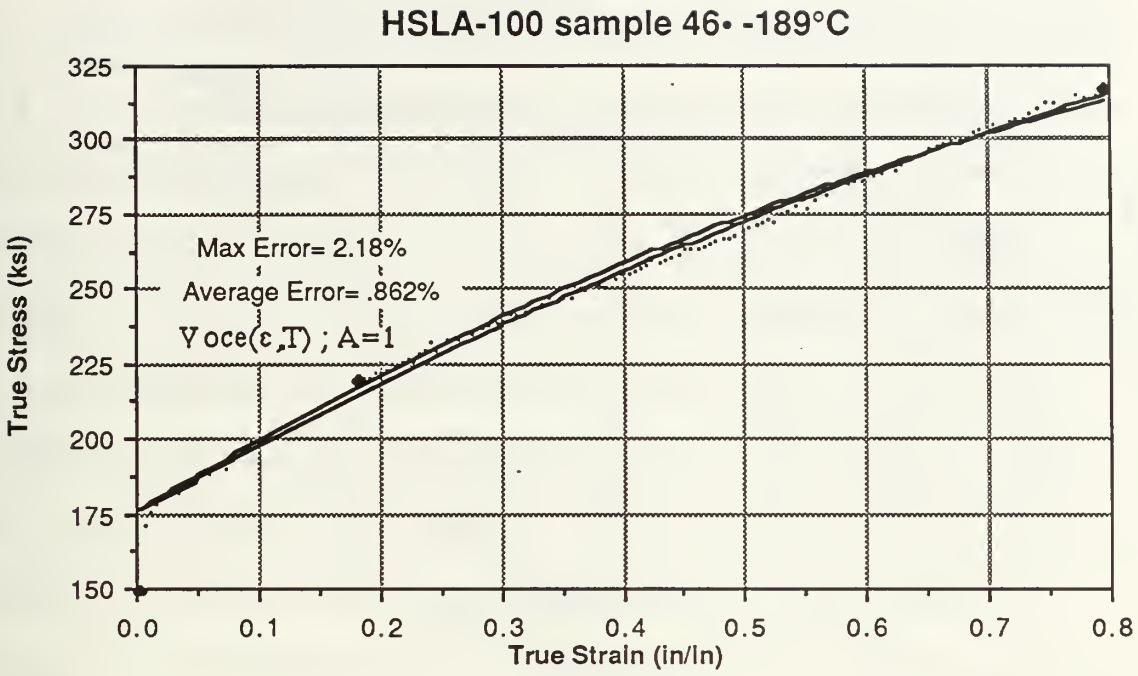

(a.)

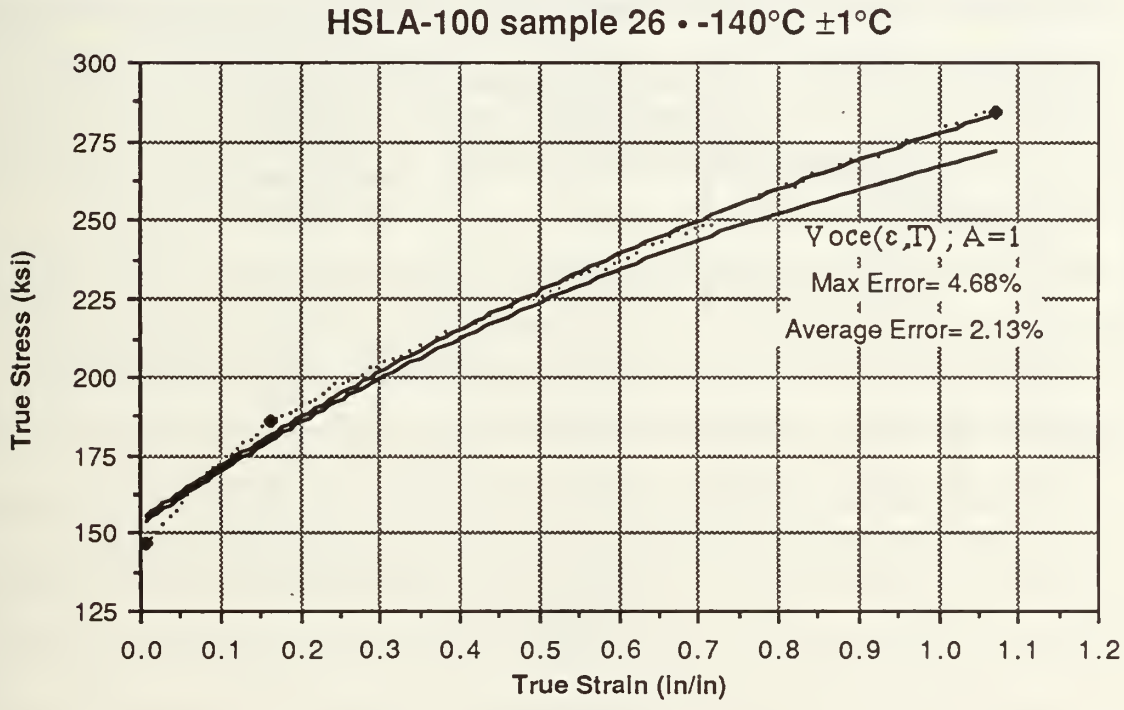

(b.)

Figure 18
Final Voce(ϵ,T) Comparison Plots

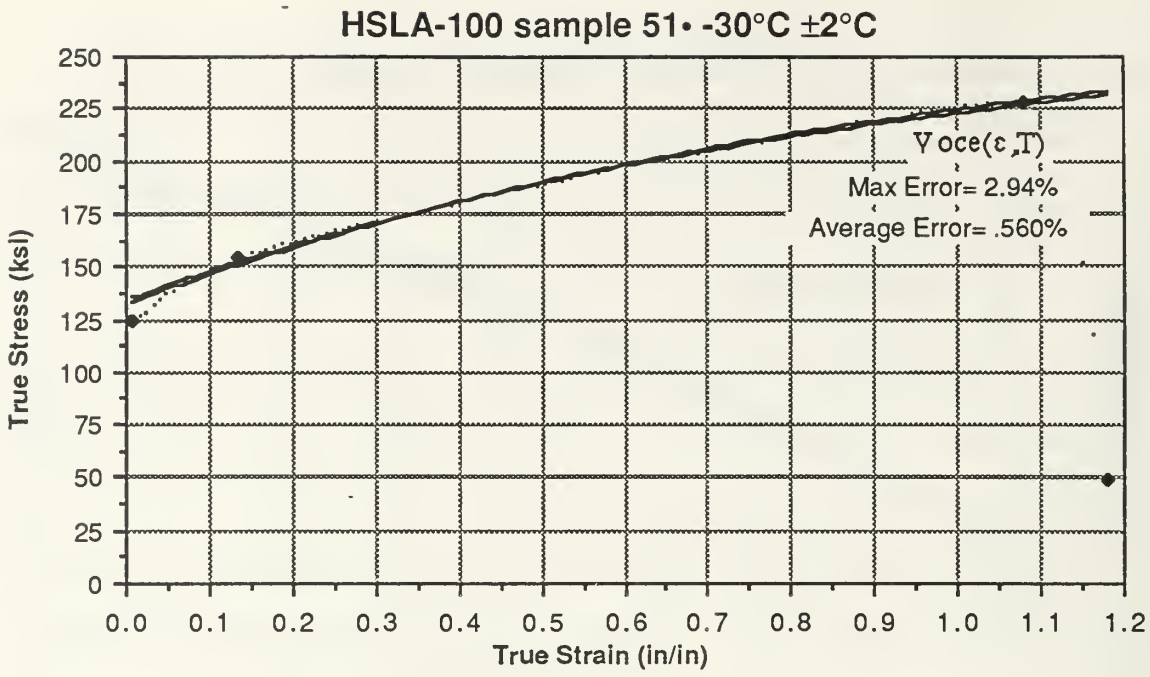

(c.)

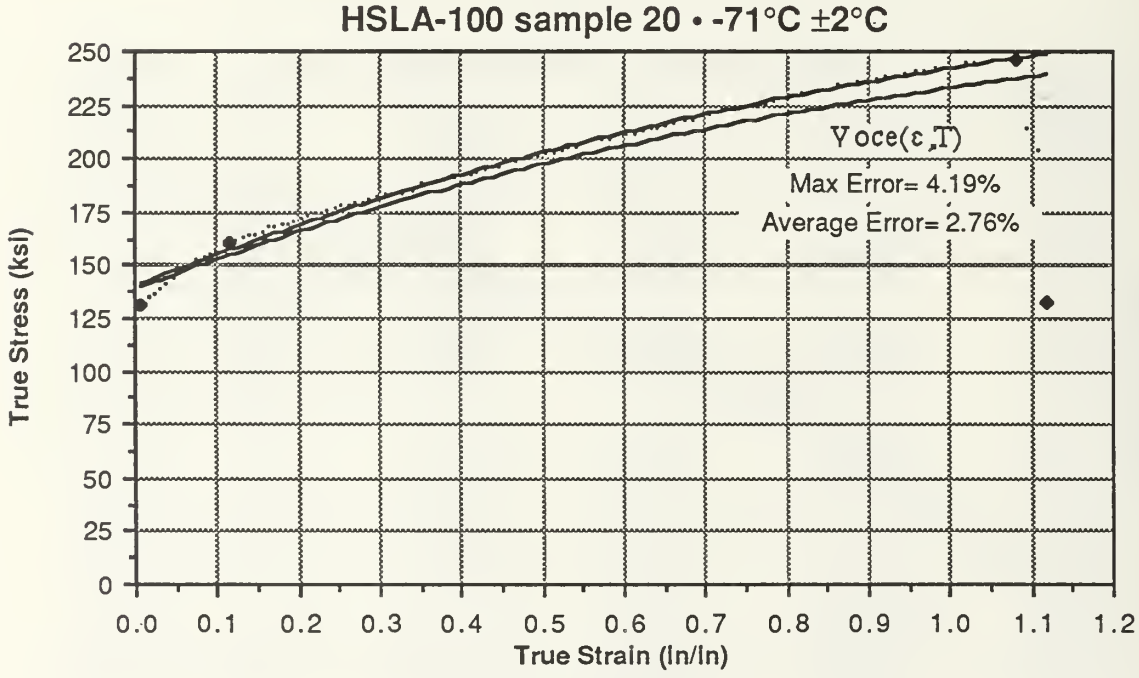

(d.)

Figure 18
Final Voce(ϵ,T) Comparison Plots

Looking at the Voce equation fit to the data, there appears to be three regions where the fit is poor. The low strain region of all tests is generally the region where the fit is the worst; the Voce curve always overestimating. The second region where the curve fit is poor is at the maximum load point where the stress is generally predicted lower than the observed values. The last region is the very high strain region of the curve near failure. In this region the prediction is higher than actual because of the rapid drop in load as the specimen fails. It is not possible to just change the value of S_∞ or So to an observed value without changing the value of the characteristic strain because of the close interaction of the coefficients. It is possible to obtain better results in all of these areas by splitting the stress/strain curve into two regions, one from the yield point to the maximum load point and another from the maximum load point to failure. Because of the desire to obtain a single equation describing stress as a function of strain and temperature this path was not pursued in great detail. However the data suggests that there may be a change in the controlling strain hardening mechanism near the point of maximum load.

D. BRIDGMAN CORRECTED TRUE STRESS VERSUS TRUE PLASTIC STRAIN

The Bridgman correction is a stress correction factor which corrects for the triaxial stress state that is generated in the neck of a tensile sample. Since the necking phenomenon begins at approximately the point of maximum load the correction becomes greatest in regions past the maximum load point. In the derivation of the correction factor, Bridgman was able to describe the correction in terms of some relatively easy to measure parameters of the tensile specimen, the diameter of the specimen at the minimum diameter and the radius of curvature in the neck. The Bridgman correction factor is given as:

$$\sigma / \sigma_{Av} = 1/[(1 + 4R_c/D) \, Ln(1 + D/4R_c)]$$

where σ is the Bridgman corrected stress and is always lower than the measured stress, σ_{Av}. R_c is the radius of curvature of the neck and D is the minimum diameter of the neck. [Ref. 13]

Sample number 43 was interrupted during testing at several intervals past the maximum load point and the instantaneous diameter and radius of curvature measured. Several methods for measuring the radius of curvature were tried including projecting the sample image and using a circle template to find a radius proportional to the known diameter of the specimen. Another method, the use of a machinists radius gage set was less successful because the gage could not fit between the grips. The most successful method, especially at low temperatures was to use a drill bit index. By back lighting the specimen the best radius fit could be found at temperatures above 0°C. At low temperatures the frost which formed on the specimen melted when touched by the drill bit, so the largest bit which melted all the frost through the neck was the diameter of the neck. Drill bits incremented in 1/64 inch gives radii accurate to 1/128 of an inch or about .008 inches. Another advantage of the drill index method is that it is not as subjective as the projection method, the drill index can measure with a smaller increment size than a radius gage set again making it more accurate.

The plot of all of the Bridgman correction data collected and the equation of an computer generated polynomial fit are shown in Figure 19. Since the tests were conducted at a constant displacement rate, the diameter change is constant and the change in radius of curvature must be responsible for the more rapid changes in the Bridgman correction near the maximum load point and again near failure.

Applying the correction to the actual data was accomplished by knowing the maximum

load for a particular test and the strain at that particular point; all strains past the necking strain were calculated and the Bridgman correction calculated from the equation shown in Figure 19. For strains prior to necking the diameter was changing and the radius of curvature was assumed to remain constant. Although this is known not true in fact, the correction factor remains relatively constant for increases in radius of curvature so this is a good approximation prior to necking. Converting the true strain into true plastic strain is accomplished by subtracting the elastic strain from the total strain.

$$\epsilon_p = \epsilon_t - \sigma / E$$

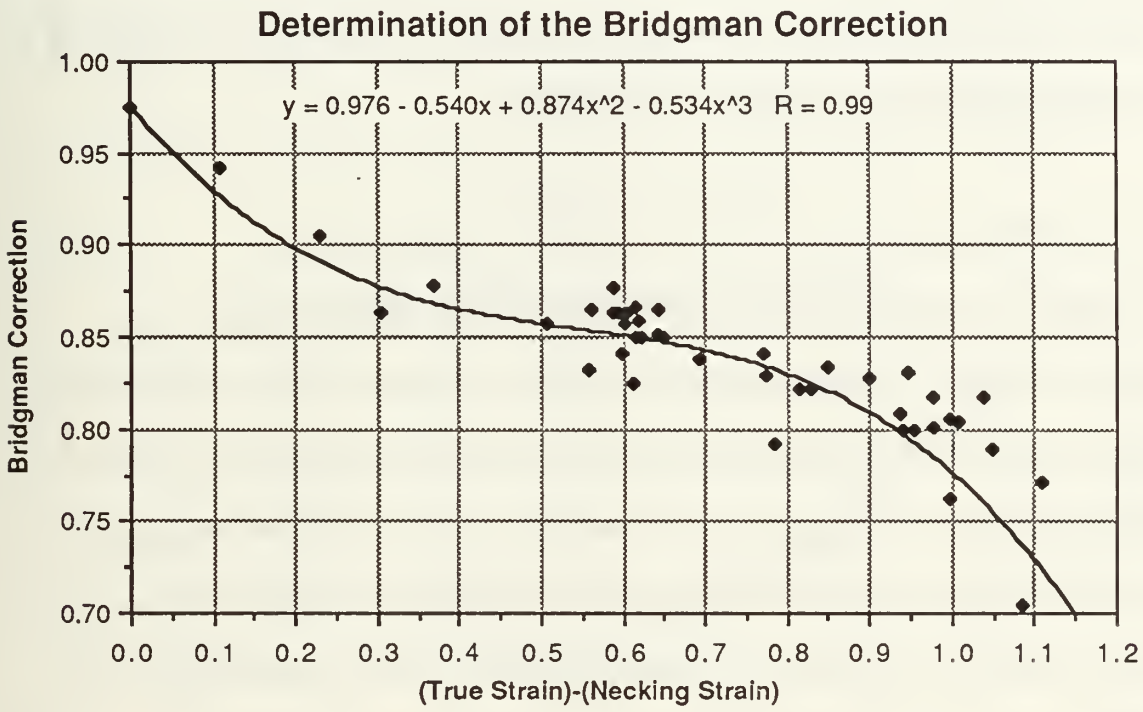

Figure 19
Collection of all Bridgman Correction Data Points for HSLA-100 Tests

Applying these corrections to an actual test yielded results shown in Figure 20. On these plots the change in slope at the maximum load point is much more obvious. On the logarithmic plot, there appears to be two separate and overlaying exponential plots

intersecting at the maximum load point. Toward the high strain regions of the curve the stress is dropping off, showing as a hook in the logarithmic plot, another unexpected result. For the single Voce equation fit for this curve, the correlation was .97; a large decrease in the accuracy of the prediction.

The Bridgman correction factor for all tests are close to the prediction curve used so the confidence in the Bridgman Correction factor, as it was predicted and used, is high. The true plastic strain is too straightforward to account for the deviations observed. There was no observed reason during the testing which could describe the rapid change in stress carrying ability at the maximum load point and then again near failure. The Bridgman correction was not given any further consideration because it is felt that it is not properly correcting for the triaxiality effects on the true stress of this material.

E. MECHANICAL PROPERTIES OF HSLA-100 WITH TEMPERATURE

Ductility, 0.2 percent yield strength, and ultimate tensile strength are more conventional material properties specified in metals specifications. For this HSLA-100 the ultimate tensile strength was to be recorded for information purposes only, the 0.2 percent offset yield strength was to be between 100 and 120 ksi, and the minimum reduction in area was to be 45 percent. The HSLA-100 used in this research showed many of the expected trends with regards to temperature. A tabular compilation of these results are provided in Table 5.

1. 0.2 Percent Offset Yield Strength

The 0.2 percent offset yield strength is one characteristic which showed a wide degree of variability in testing. The results of all tests are shown in Figure 21. In most tests, the yielding behavior of this steel was such that load/displacement curve rounded off

slightly as the yield point was approached and then leveled off to horizontal for a short period in what may have been a second yield point for the material.

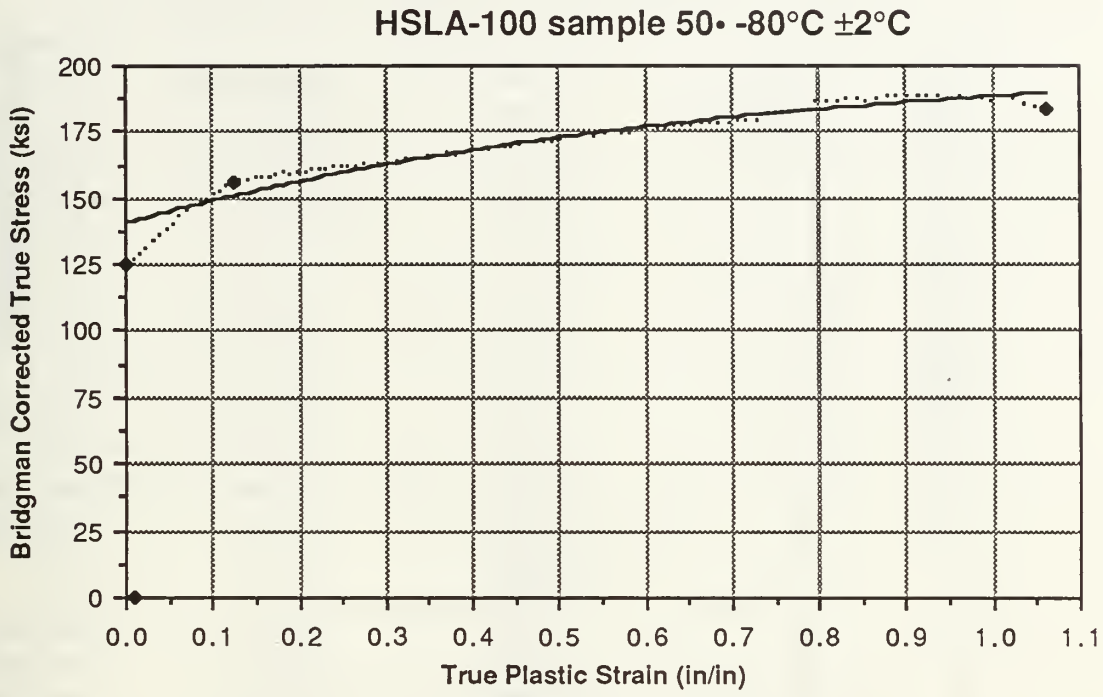

(a.)

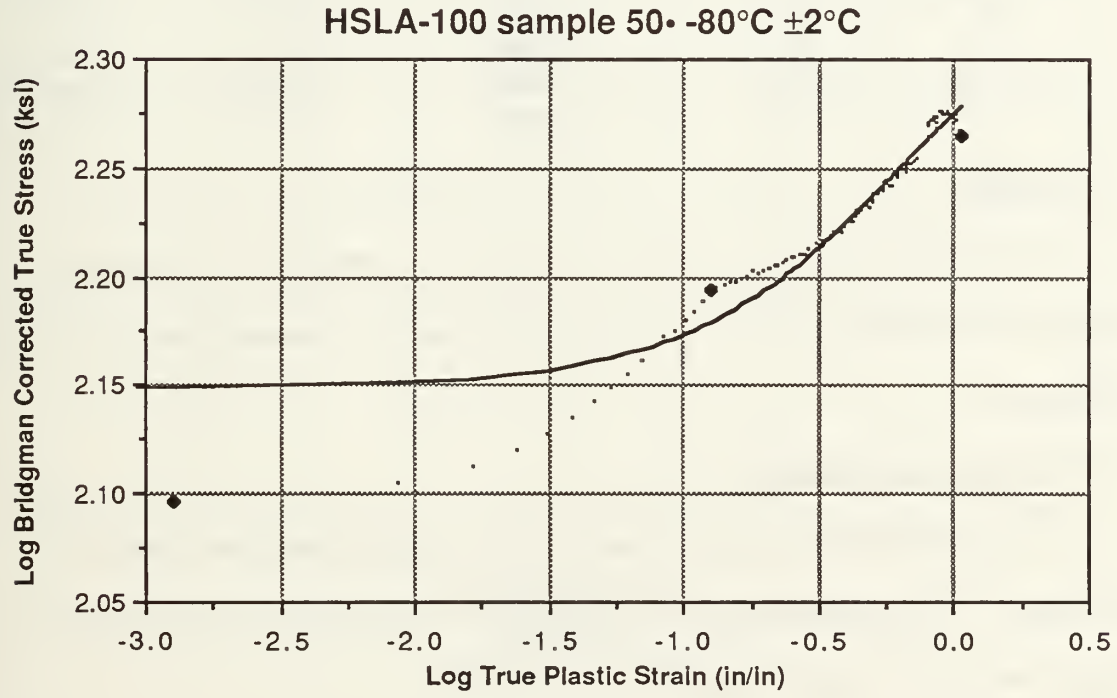

(b.)

Figure 20-Bridgman Corrected True Stress versus True Plastic Strain Plots

TABLE 5
MATERIAL PROPERTIES OF HSLA-100

Temp (°C)	Sample number	Ductility ΔA/A	0.2 percent σ_y(ksi)	Ultimate Tensile Strength(ksi)
-189	46	.5215	151.6	219.2897
-176	28	.5977	140.3	195.8169
-170	52	.5701	139.4	198.1512
-154	34	.6217	145.4	181.4601
-150	47	.599	145.5	180.9536
-140	26	.6551	136.3	185.6136
-133	25	.6168	124.3	183.7
-132	37	.6198	135.3	172.8383
-124	24	.6799	141.5	179.9
-117	19	.6578	113.4	169.6990
-110	49	.6467	124.3	169.9216
-101	23	.6643	134.3	171.0
-91	22	.6643	124.3	160.1
-80	50	.6794	121.3	160.3666
-71	20	.6670	119.3	161.5373
-56	31	.6766	122.3	155.6384
-30	51	.7173	120.9	154.3026
0	30	.7095	116.3	152.7214
18	36	.6898	122.3	149.5627
18	35	.7130	119.3	144.0150
37	27	.7037	105.6	140.9909

2. Ductility

The ductility, measured by reduction in area (ΔA/A), of the HSLA-100 is shown in Figure 22. The ductility was lowest at low temperatures with a minimum reduction in area of 52 percent.

3. Ultimate Tensile Strength

The true stress at the maximum load point is shown in Figure 23 as a function of temperature. This data exhibit the expected changes with temperature, increasing tensile strengths as the temperature decreases.

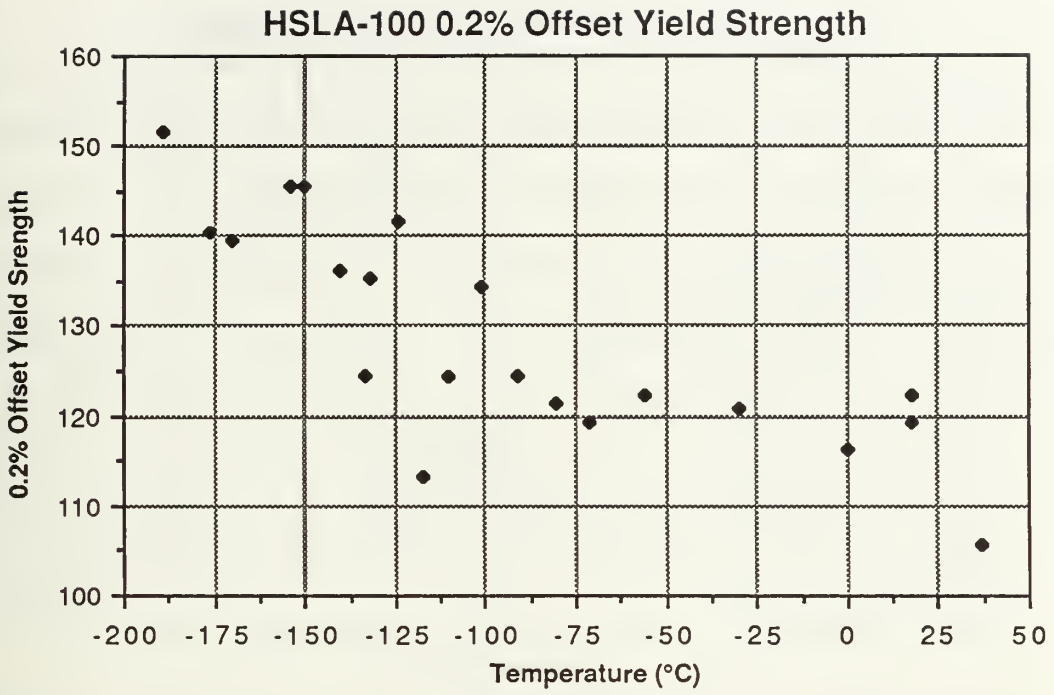

Figure 21
0.2 Percent Offset Yield Strength

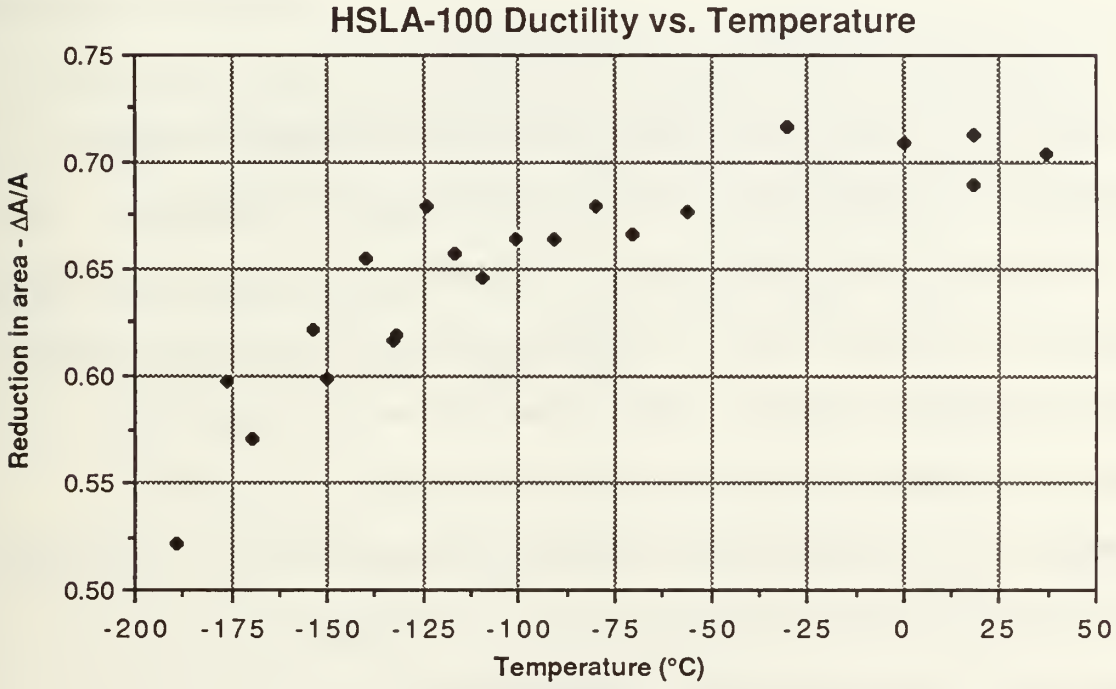

Figure 22
Ductility of HSLA-100

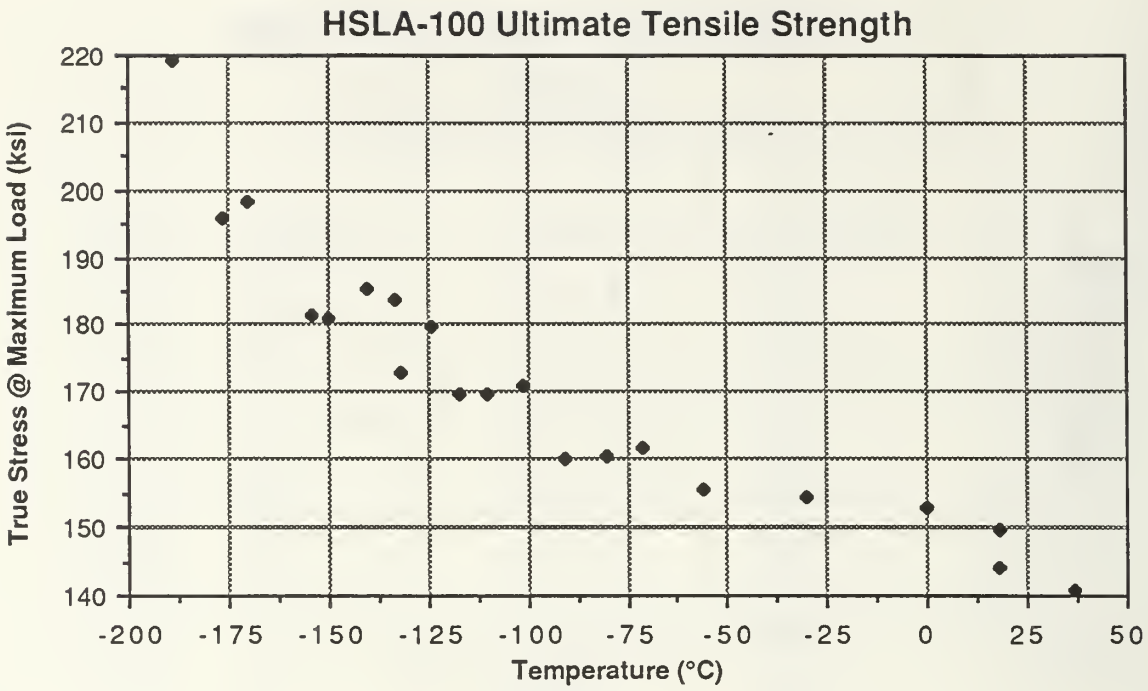

Figure 23
HSLA-100 Ultimate Tensile Strength

F. FRACTURE CHARACTERISTICS AND METALLOGRAPHY

Fractographic studies of the macroscopic and microscopic features of the fracture surfaces were conducted using light microscopy and scanning electron microscopy.

The most notable macroscopic feature of the this material was the sequence of events during the failure process. Stated in a straightforward manner, only two of the 11 samples tested at temperatures from -56°C to -140°C fractured into two pieces during actual testing. In this temperature range and below the first fracture was a vertical split or delamination in the neck and running for a total length of about 1/4 of an inch. A photograph of one of these splits is shown in Figure 24. In a few of the samples there were perpendicular vertical splits, but in all cases there was one major split. For all of these samples there was the loud pop associated with a sample failure but the sample remained intact. The deformation in this temperature range, at this point, is presumed to have

occurred in a jump since the tests were terminated by the MTS controller due to the error between control and actual displacement voltages becoming too large. Metallographic examination of the split shows that it is parallel to the banding noted in the microstructure. Figure 25 is a photograph showing the microstructure and its orientation with the split.

From the geometry of the sample, all plastic deformation is restricted to a small length in the center of the sample. The actual length of localized deformation depends on the yield strength, strain hardening, ultimate tensile strength and initial diameter of the sample. With the radius of curvature of the hourglass portion equal to 1.1 inches, the plastic deformation occurs in the center 0.20 to 0.25 inches of the initial sample. Looking at the sample and measuring from the base of the hourglass portion (the elastic region of the sample) the splits appear to end at about the location of the boundary between elastically and plastically strained material.

Fracture profiles of Figure 26 show some specimens tested in the transition region of -140°C to -189°C. The fracture surfaces perpendicular to the load of all tests except that at -189°C appear to have occurred at about the location of the elastic-plastic boundary. At this point it is also noted for samples 26 and 47 in Figure 26 (b) (-140°C and -150°C) that there was failure both in and outside of the neck.

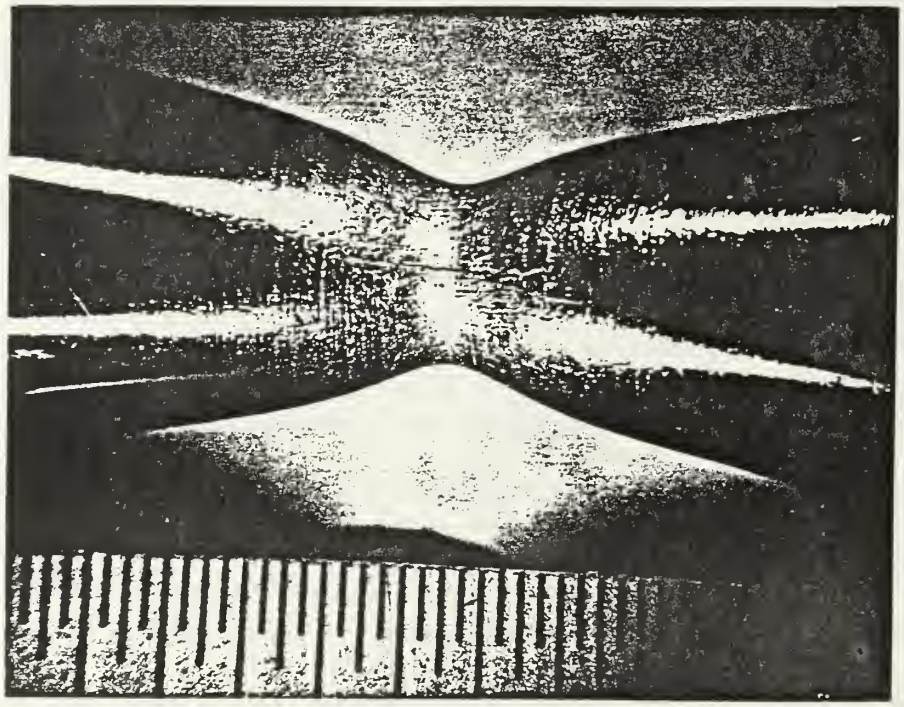

Figure 24
HSLA-100 Sample 19 (-117°C) Vertical Split
1 Ruler Division = 1/64 inch

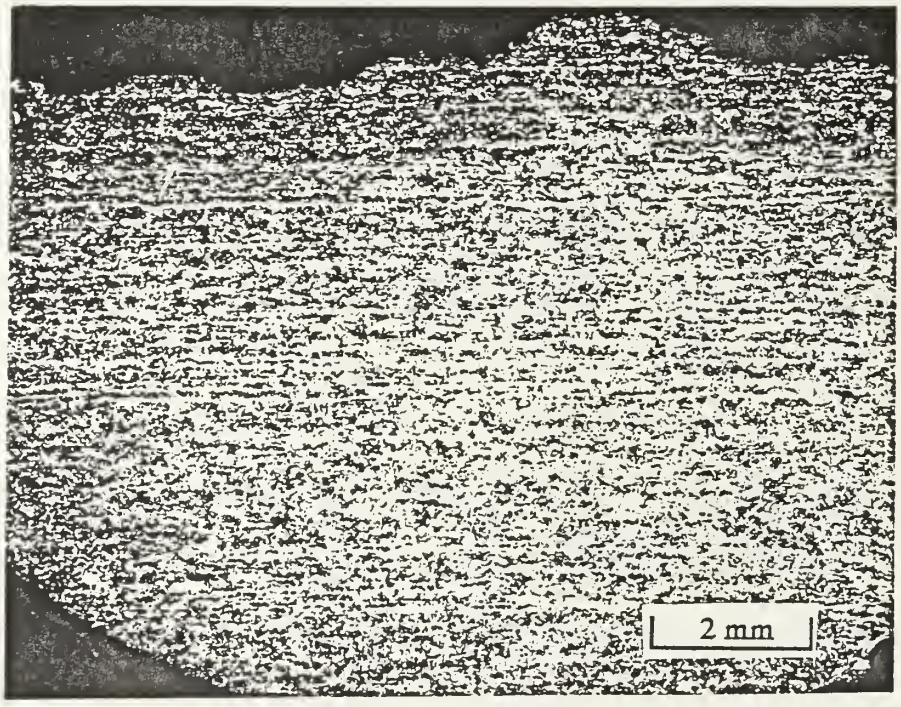

Figure 25
HSLA-100 Sample 52 (-170°C) Cross Section of Neck

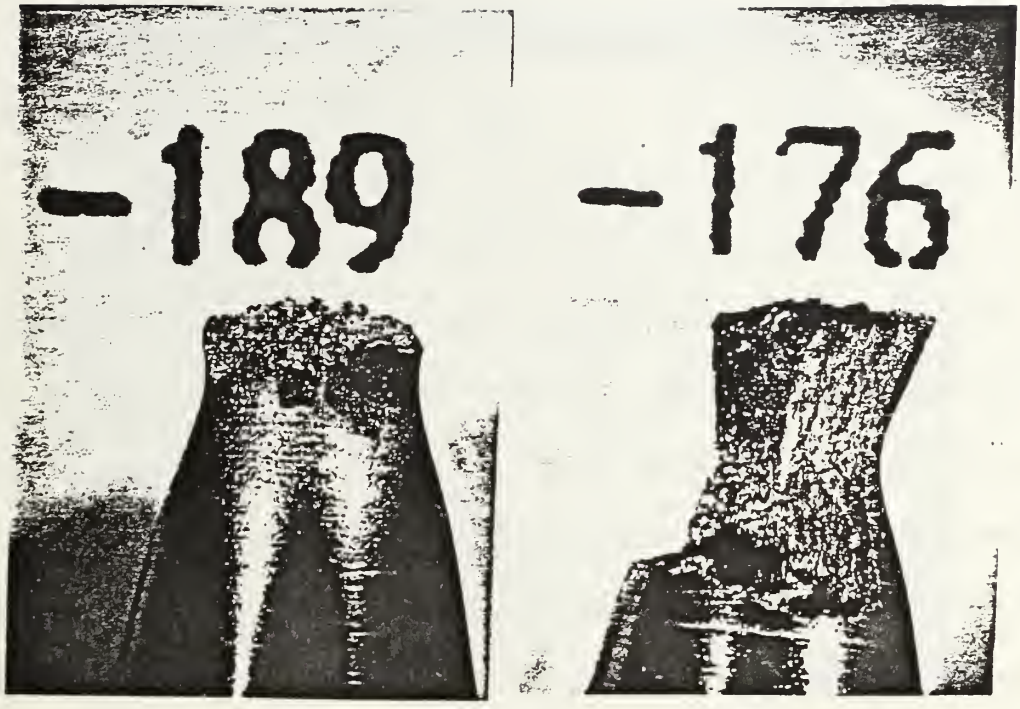

(a.)

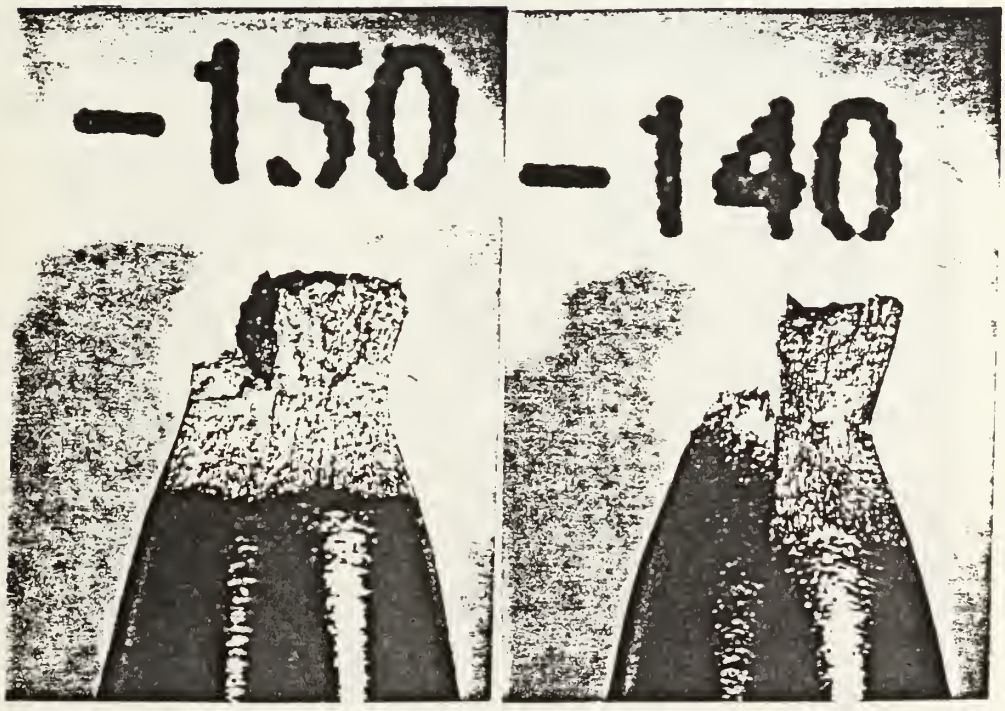

(b.)

Figure 26
Fracture Profiles

Scanning electron microscopy observations on the fracture surfaces shows many important features which can be linked to the fracture profiles. The various views of the fracture surfaces are shown in Figure 27. At temperatures from room temperature to -30°C the typical cup and cone of ductile fracture were noted, with the appearance of early stages of delamination. The higher magnification photographs show some of the sites where microvoid coalescence was initiated. At -71°C the area of delamination has opened up and the cup and cone surface is no longer evident. At -101°C the surface has taken on a jagged appearance and the high magnification photograph shows a still predominantly ductile fracture surface with small regions of quasi-cleavage. At -140°C and -150°C the mode of failure was dependent on the the location of the fracture surface relative to the neck. In the areas where the failure was out of the neck, the fracture surface was brittle (cleavage) and in the areas where it was in the neck , the surface was all ductile. Below this temperature all of the fracture surfaces were out of the neck, except for the test at -189°C. At -189°C there also appeared to be more ductile areas on the fracture surface than the surfaces at immediately higher temperatures although the fracture was still predominantly brittle.

Figure 27(a.)
Sample 30 (0°C) Fracture Surface, Low Magnification

Figure 27(b.)
Sample 51 (-30°C) Fracture Surface, Low Magnification

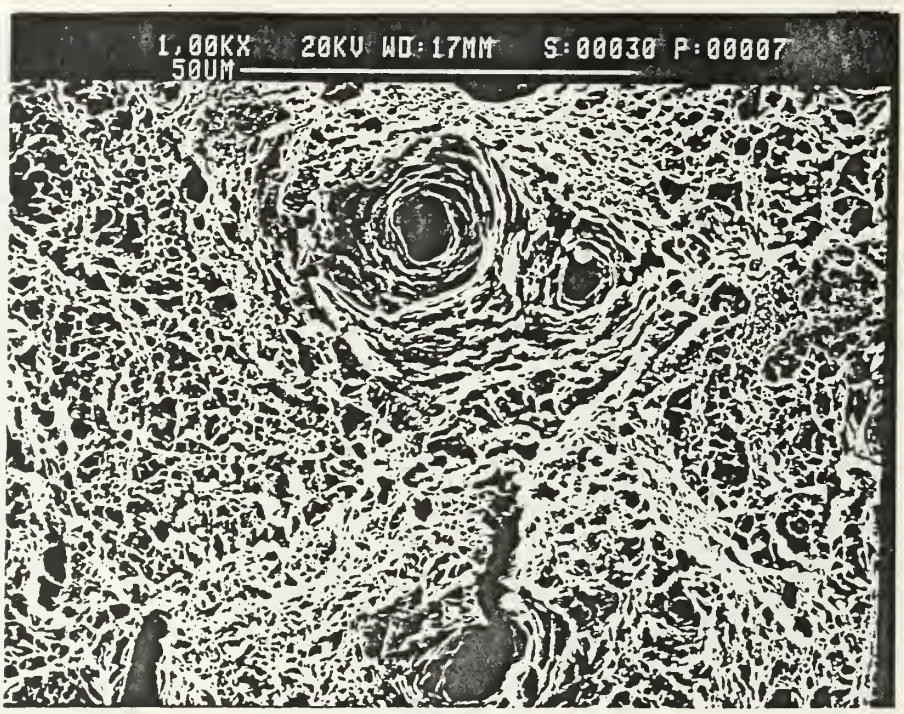

Figure 27(c.)
Sample 30 (0°C) Fracture Surface, High Magnification

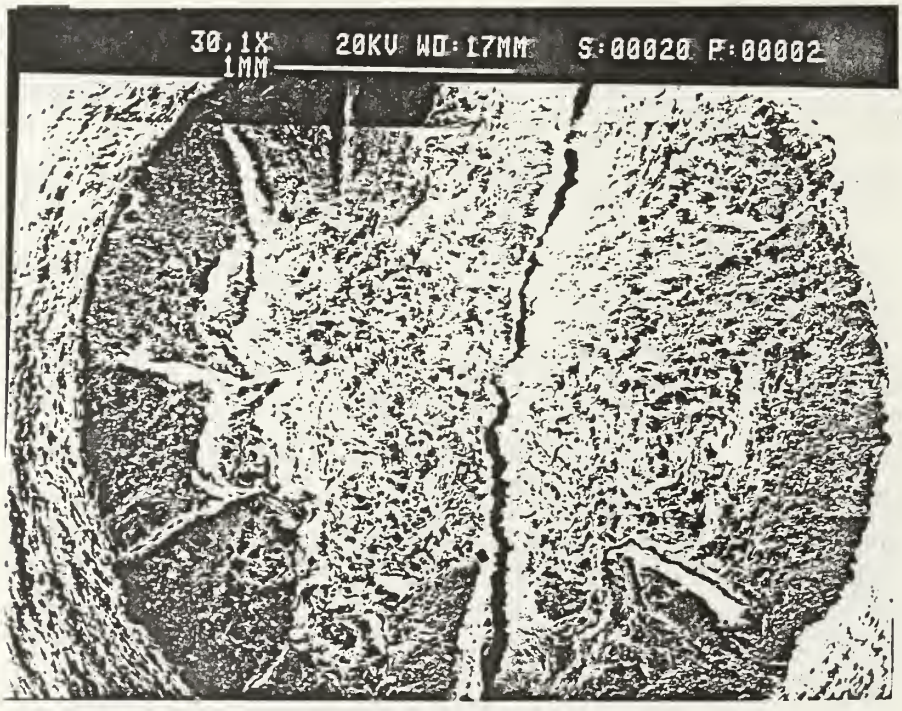

Figure 27(d.)
Sample 20 (-71°C) Fracture Surface, Low Magnification

Figure 27(e.)
Sample 23 (-101°C) Fracture Surface, Low Magnification

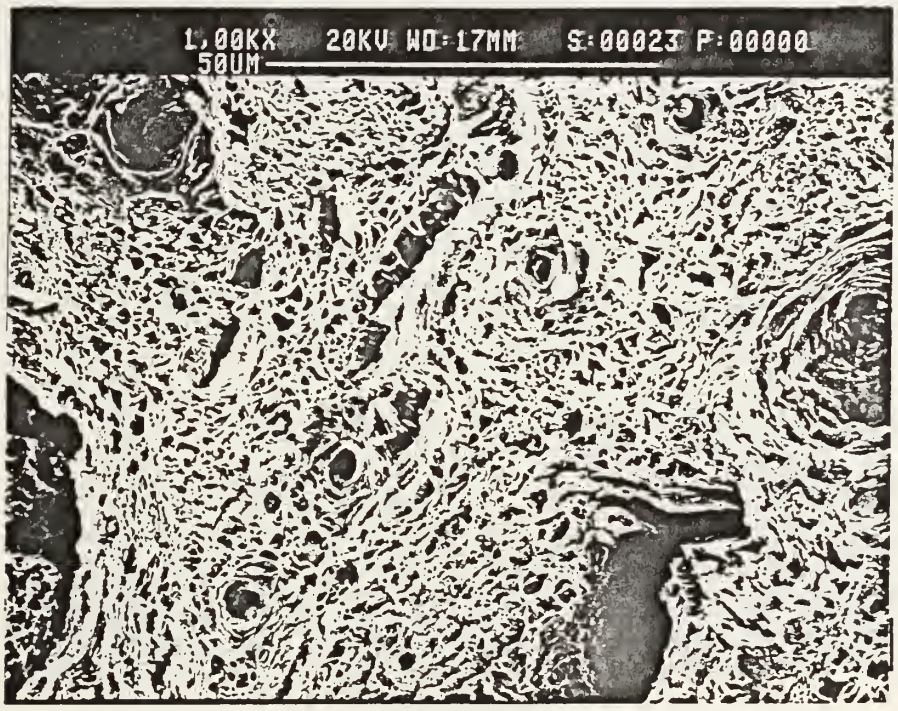

Figure 27(f.)
Sample 23 (-101°C) Fracture Surface, High Magnification

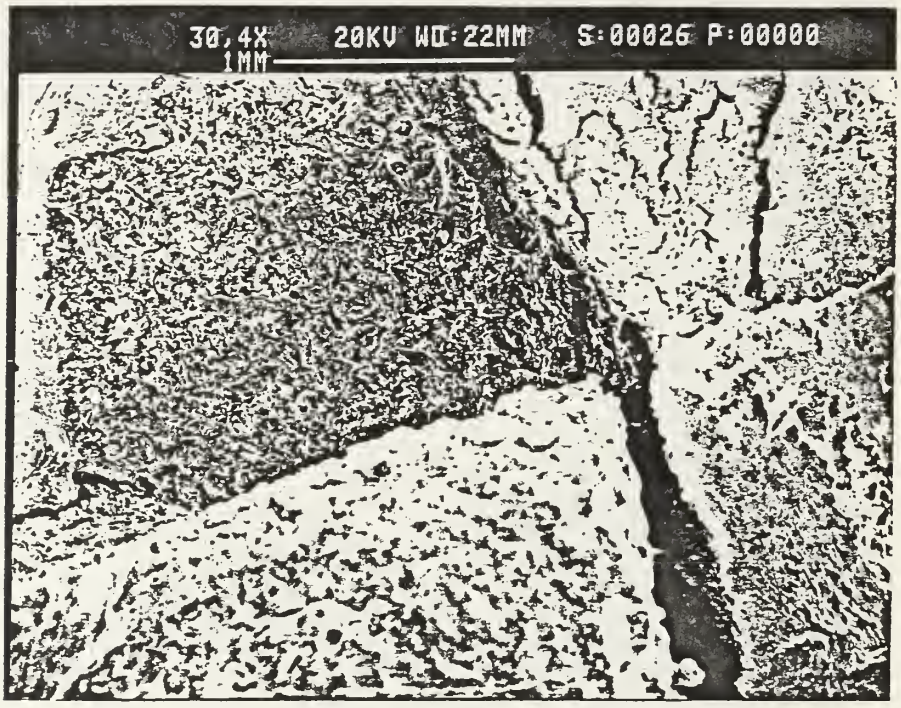

Figure 27(g.)
Sample 26 (-140°C) Fracture Surface, Low Magnification

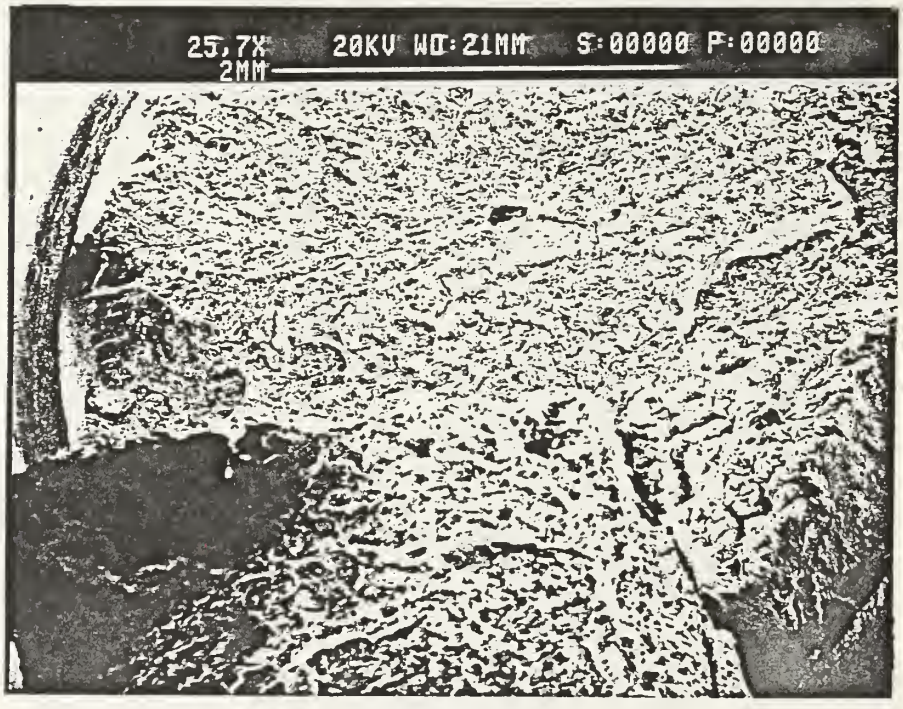

Figure 27(h.)
Sample 47 (-150°C) Fracture Surface, Low Magnification

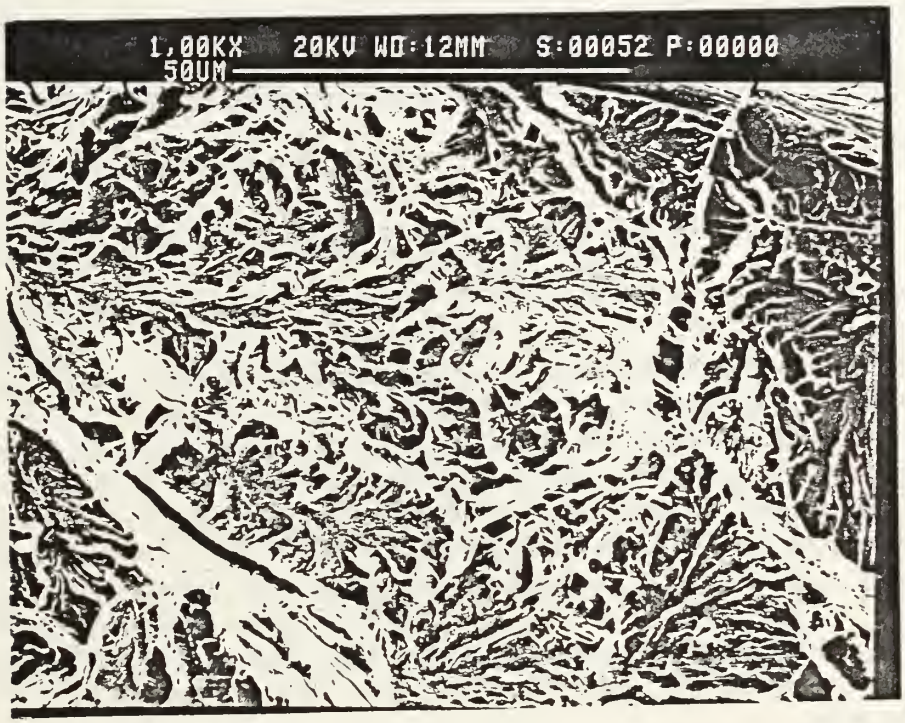

Figure 27(i.)
Sample 52 (-170°C) Fracture Surface, High Magnification

V. DISCUSSION

A. MODIFICATIONS / IMPROVEMENTS IN THE USE OF THE VOCE EQUATION

In the derivation of the constituitive Voce equation, $\sigma(\epsilon,T)$, the characteristic strain, A, was taken to be a constant equal to 1.0. This value is the average of all of the values of A obtained. Some of the variables of testing which affect its value are: which region of the stress-strain curve is being evaluated; how far the test was run toward actual failure; and how large a deviation existed in the curve about the maximum load point. There is also an intimate relationship between S_∞, So and A so that if one is changed the others also have to be changed for the curve to fit the data. The characteristic strain is believed to be a constant for this series of tests but may be dependent on the strain rate. For this series of tests the strain rate was relatively low, about 1.0×10^{-3} in/in-sec. At higher strain rates the value of S_∞ would be expected to raise, increasing the quantity $Ln(S_\infty - S)$ for a given strain. The overall effect would be to lower the slope of the strain-$Ln(S_\infty - S)$ curve, which is the characteristic strain.

There are two definite strain hardening regions for this material with a transition occurring at about the maximum load point. In an analysis of the two regions, the average value of A from the yield point to necking was 0.1829 and the average from the maximum load point to failure was 1.522 showing a large difference between the two regions. It is for this reason that the characteristic strain should not be dropped from the Voce equation describing the stress as a function of strain and temperature. Further, this suggests that future research should attempt to determine if there is a change in the strain hardening mechanism after necking occurs.

Using separate versions of the Voce equation to describe the two strain hardening regions seems initially to more accurately fit the curves with correlations of .999 occurring frequently. In order to effectively use a two region / two equation form of solution, the transition point must be accurately predicted also. For the case of the Voce equation and HSLA-100 this point is the maximum load point. Reference 12 points out that the slope of the stress/strain curve at the maximum load point equals the true stress at that point. Based on this fact and using the derivative of the Voce equation for the conditions of maximum load the stress at maximum load is described by the equation:

$$d\sigma/d\epsilon = \sigma_{\text{max load}} = S_\infty/(1 + A)$$

and for the case of A= 1 the stress at maximum load = $S_\infty/2$. The stresses calculated using this equation and the actual ultimate tensile strengths found experimentally are plotted in Figure 28. The individual Voce equation coefficients for the test and the general Voce coefficients as a function of temperature are all significantly lower than the actual values with the worst results near room temperature.

From the experimental results it is known that the predicted value of stress at the maximum load point is always low but this also raises a question of confidence in the Voce equation for describing actual material behavior. The Voce equation does fairly accurately describe the stress/strain behavior of HSLA-100 but there are material inconsistencies observed and not fully explained by this equation. If this problem of the transition/maximum load point can be resolved, then the Voce equation or one of its derivatives could be used very well to predict the behavior of HSLA-100 in terms of true stress/true strain. For one test, the two region Bridgman corrected curve was fit and is shown in Figure 29. The results appear to be very good except at the very end in the

vicinity of the hook, where the sample is starting to fail.

B. SAMPLE GEOMETRY RELATIONSHIP TO FRACTURE

The hourglass specimen was used to localize the deformation in the specimen enabling the true stress state to be accurately determined through necking up to fracture. Fracture characteristics such as splitting only in the plastic region and final fractures near the elastic-plastic interface bring rise to questions of the applicability of information obtained from hourglass specimen tests. However, preliminary tensile tests using uniform gage samples at David Taylor NSRDC have fractured in an identical fashion as these hourglass specimens.

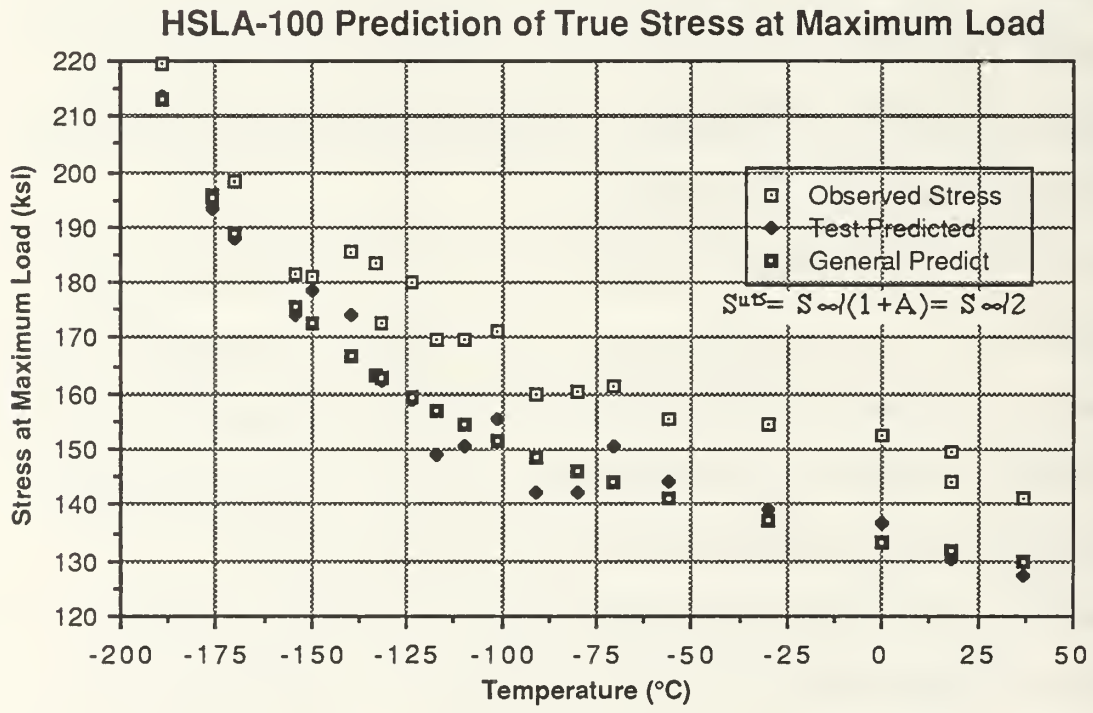

Figure 28
Prediction of the Ultimate Tensile Strength

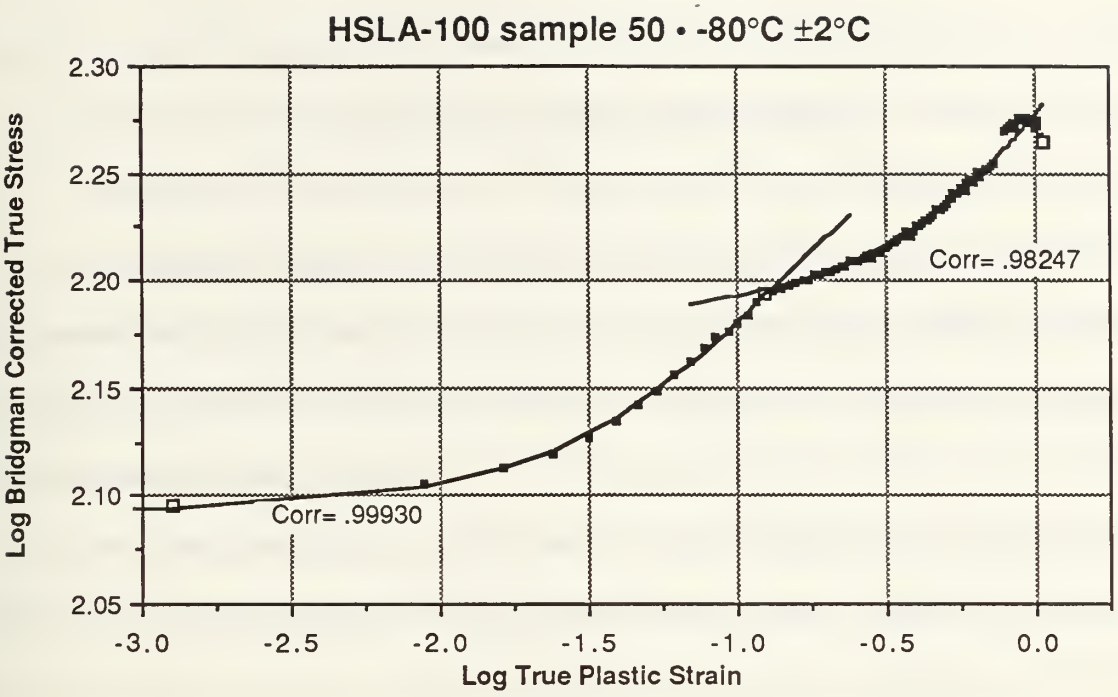

Figure 29
Two Curve Fit for the Bridgman Corrected True Stress / True Plastic Strain

The aspect of the fracture that is most puzzling is the fact that all cleavage fractures occurred outside of the neck where the nominal stress is much lower than in the neck. It appears that the large plastic strain experienced within the necked region has raised the cleavage stress. All fractures in the neck occurred by microvoid coalescence while all fractures outside the neck occurred by cleavage. Some samples in the transition temperature range exhibited regions of ductile fracture in the neck and brittle fracture outside the neck. The effects of large prestrains on cleavage fracture should be the topic of future research.

The rapid increase in strength with decreasing temperature indicates that the Peierls-Nabarro stress is an important component of the strength of this alloy, especially at low temperatures. Thus, the exponential equation describing the temperature dependence of the strength coefficients, So and S_∞, in the Voce equation should be, at least, correct in

form. The characteristic strain, A, in the Voce equation is a measure of the strain hardening rate of the material. Considerable scatter in the value for A was found, but no evidence of any temperature dependence of A was observed. This indicates that the mechanism controlling the strain hardening in this alloy is probably independent of temperature. However, the fact the stress-strain curve has what appears to be different strain hardening regions before and after the maximum load may indicate that the controlling mechanism changes once a critical strain is exceeded. If this is the case then a single constituitive equation like the Voce equation will need to be modified to reflect the change in the strain hardening mechanism. However, the single Voce equation which incorporates the effect of temperature appears to produce a very adequate description of the stress-strain behavior of this alloy at this quasi-static strain rate.

VI. CONCLUSIONS AND RECOMMENDATIONS

The Voce equation is quite accurate in describing the the tensile behavior of HSLA-100 steel but has some areas of weakness. In low strain regions (less than about 0.01) the Voce equation always overestimates the actual stress. The Voce equation also underestimates the stress at the point of maximum load.

Taken as a function of temperature, the value of A appears to be a constant; however the temperature dependence of So and S_∞ are accurately described by an exponential function of the general form:

$$S = Co + [C1 * \exp(Tc/T)]$$

where Co, C1, and Tc are constants and T is the temperature of the test in degrees Kelvin (°K). Using least squares curve fit of observed data to the equation, the coefficients are defined as follows:

$$So = -5148.559 + [5261.393 * \exp(1/T)] \quad (ksi)$$

$$S_\infty = -78.80511 + [292.1489 * \exp(46/T)] \quad (ksi)$$

$$A = \text{constant} = 1.0 \quad (in/in)$$

These equations can be substituted into the Voce equation to form a constituitive equation for the true stress in HSLA-100 at low strain rates as a function of strain and temperature:

$$\sigma(\epsilon,T) = S_\infty(T) - [(S_\infty(T) - So(T))\exp-(\epsilon/A)].$$

Recommendations for further study include evaluating the effect of higher strain rates on the stress coefficients of the Voce equation with particular attention to the characteristic strain. A data acquisition system for such experiments should in addition to monitoring the load, should simultaneously be able to measure the the detailed plastic flow in the region of

the neck. The use of a bit mapping scheme or diffraction of laser beams may work well. This is important to be able to more accurately predict the actual triaxial stress correction and the corresponding stress state in the neck. The mechanism of deformation and the effect of prestrain on cleavage fracture also need further study.

Another topic poorly understood is the effect of the delamination or splitting, on the stress state in the necked region of the test specimen. Cleavage fractures always initiated transverse to the loading direction at the end of the axial split, a region of much lower stress than in the neck for these hourglass samples. Why does the material exhibit cleavage here instead of in the neck where the stresses are much larger ?

APPENDIX A

INTERIM SPECIFICATION FOR TRIAL COMMERCIAL PRODUCTION OF HSLA-100 STEEL PLATES

Melting, Refining and Casting

The heat shall be fully killed and produced to fine grain practice. It shall be made with a low sulfur practice, vacuum degassed and argon injected with CaSi or Mg for sulfide shape control. The heat shall be ingot cast with bottom-pour molds to insure good surface.

Chemical Composition

The Chemical composition shall be as shown in Table I.

Element	Target for First Heat	Max. % by Weight Unless a Range is Indicated
Carbon	0.04	0.06
Manganese	0.90	0.75 - 1.05
Phosphorus	ALAP*	0.015
Sulfur	ALAP*	0.006
Silicon	0.25	0.40
Nickel	3.5	3.35 - 3.65
Chromium	0.60	0.45 - 0.75
Molybdenum	0.60	0.55 - 0.65
Copper	1.60	1.45 - 1.75
Columbium	0.025	1.45 - 1.75
Aluminum	0.030	0.020 - 0.040
Nitrogen	0.010	0.015

* As Low As Possible

Hot Rolling

Plates 1/4, 3/4, 1-1/4, and 2 in. thick shall be rolled. Extra care shall be taken to minimize rolled-in scale that could interfere later with achieving an adequate cooling rate

during quenching from the solution treating temperature. The plates shall be roller leveled while still warm after rolling.

Heat Treatment

All of the plates shall be solution heat treated for one hour at 1650°F and platen quenched with high pressure water jets from above and beneath the plate. The quench water shall not exceed 100°F to ensure an efficient quench.

The plates shall be given an age hardening treatment using temperatures and times determined for each plate by preliminary tensile testing of samples from cupons aged at various conditions. Aging conditions for the plates shall be chosen so as to give the tensile properties listed in Table II.

Mechanical Properties

The heat treated material shall meet the tensile property requirements specified in Table II and the impact property requirements specified in Table III.

Table II Tensile Properties

Ultimate Tensile Strength, psi	To be Recorded for Information Only	
Yield Strength, 0.2% Offset, psi	≤0.75 in. 100,000 to 120,000	>0.75 in. 100,000 to 115,000
Min. Elongation in 2 in., %	17	18
Min. Reduction in Area, Round Specimen, %	- -	45

The tensile properties shall be determined as the average value of duplicate specimens from each plate tested in accordance with ASTM method of testing E8. Full thickness flat specimens shall be tested for the 1/4-in. thick plate and standard round specimens 0.505

in. diameter shall be tested for the plates 3/4 in. thick and thicker. All specimens shall be taken tranverse to the primary rolling direction.

Table III - Impact Properties

Test	Plate Thickness in.	Specimen Size	CVN Test Temp., °F	Energy,[a] ft - lb
Charpy V-Notch Tranverse	0.25	5 mm x 10 mm	0 ± 3	28
			-120 ± 3	15
	0.75, 1.25, 2.00	10 mm x 10 mm	0 ± 3	55
			-120 ± 3	30

[a] Avg. of three tests, minimum.

The Charpy impact properties shall be determined in accordance with ASTM method of testing E23. Three tests transverse to the final rolling direction of the plate shall be conducted. No single value shall fall below the minimum average specified in Table III by more than 5 ft-lb for standard specimens and 2-1/2 ft-lb for half size specimens.

APPENDIX B

BASIC Computer Program for Calculation of Voce Equation Coefficients

```
REM** THIS PROGRAM IS TO TAKE LOAD/DISPLACEMENT DATA FROM A DATA
REM** FILE, PUT IT INTO ARRAYS AND THEN CALCULATE THE VOCE EQUATION
REM** COEFFICIENTS.  VERSION 1.3 USES TRUE STRESS VS TRUE STRAIN
REM**
REM**  This program is written for the Apple Macintosh PC in Microsoft BASIC
REM** Version 3.0
'*************************************************************
'   REFERENCE:  Fatigue, Tensile, and Relaxation Behavior of Stainless Steels;
'         by J.B. Conway, R.H. Stentz, and J.T. Berling; 1975 by Technical
'         Information Center, Office of Information, United States Atomic Energy
'         Commission.
'*************************************************************
'Major variables used in the program:
'      A1    Instantaneous cross sectional area
'      CORR    Local maximum correlation for a pass
'      CORRMAX    The maximum correlation found for the data points
'      D0    Initial sample diameter
'      DISP    Diametral displacement
'      LOD    Load
'      MAXLOD    Load at UTS
'      MAXLODPT    Number of the data point of the max load
'      R    Correlation
'      SINF    Incremented S-infinity
'      SINF0    Value of S-infinity for the maximum correlation
'      S0    Load where plastic deformation begins≈ the 0.1% yield strength
'      STRAIN    True strain
'      STRESS    True stress
'      STRESSU    Ultimate tensile strength
'*************************************************************
REM**
REM**              S= S∞ -(S∞ - So) e^-(strain/A)
REM**
REM**    THE METHOD OF SOLVING THIS EQUATION IS AN ITERATIVE ESTIMATION
REM** OF S∞ UNTIL THE PLOT OF Ln(S∞-S) vs STRAIN (SEMILOG PLOT) IS FOUND
REM** TO BE MOST LINEAR BY THE HIGHEST CORRELATION COEFFICIENT.
REM**  AT THIS VALUE OF S∞, A IS THE SLOPE OF THE LINE AND
REM** THE INTERCEPT WILL GIVE THE VALUE OF (S∞-So) FROM WHICH So CAN
REM** BE CALCULATED
REM
REM** DIMENSIONING THE CALCULATION ARRAY AND INPUT OF DATA
```

```
DIM LOD(500) , DISP(500) , STRESS(500) , STRAIN(500)
NEXTFILE:
PRINT
PRINT
PRINT "Input the name of your input file name with the load/displacement"
PRINT "data in it.  The data should be in the order of  [load, displacement ] "
PRINT
PRINT "INPUT FILE NAME:";
   BEEP
   INPUT DAT$
OPEN DAT$ FOR INPUT AS #1
PRINT
PRINT
PRINT "Input the sample original diameter in inches";
   BEEP
   INPUT D0
   R0= 1.1        'Radius of curvature of the hourglass samples
   PRINT
   PRINT
PI= 3.14159
N=0
SMAX=0 : MAXLOD= 0
REM**   LOOP THROUGH TO STORE LOAD/DISP DATA IN ARRAYS FOR FUTURE
REM**   CALCULATIONS
   WHILE NOT EOF(1)
      N= N+1
      INPUT#1,LOD(N) , DISP(N)
      IF LOD(N) > MAXLOD THEN    'Looking for the point where necking begins
         MAXLOD= LOD(N)
         MAXLODPT= N
      END IF
   WEND
CLOSE #1
REM
AGAIN:
PRINT N;" sets of data have been read from file "; DAT$; " stress/strain and "
PRINT "are now being calculated."
REM       Calculation of stresses and strains
   FOR I = 1 TO N
      A1= (PI/4)*((D0 - DISP(I))^2)        'instantaneous cross sectional area
      STRAIN(I)= 2*LOG(D0/(D0-DISP(I)))  '2 x diametrial strain= longitudinal strain
      STRESS(I)= LOD(I)/A1                  'insantaneous true stress
   NEXT I
   PRINT
   PRINT "Necking begins at point ";MAXLODPT; " for load"
   PRINT
BEGINNING:
SMAX= 0
```

```
PRINT
PRINT "Enter the range of points you desire to look at using data point numbers"
PRINT "  separated by a comma.";
   BEEP
INPUT STARTPT,STOPPT
'** Looking for the max stress in the interval we are looking at
   FOR I= STARTPT TO STOPPT
      IF STRESS(I) > SMAX THEN SMAX= STRESS(I)
   NEXT I
'
PRINT
PRINT "Sums of the data are now being calculated for a best correlation fit."
PRINT
PRINT
REM    For the calculation of sums the following notations will be used:
REM    log(S-infinity - true stress) = Y, log(true strain) = X,
REM     ΣX = A# , ΣY = B#, ΣXY = C#, ΣX^2 = D#, (ΣX)^2 = A#^2 = E#, ΣY^2 = F#,
REM     (ΣY)^2 = B#^2 = G# , R= correlation
REM
CORR= 0 : CORRMAX= 0 : STP= 1    'CORR and CORRMAX are a comparitive
'     correlation FOR use with R ; STP
'    is a step size which will decrease as we narrow in on S-infinity
SINF= SMAX + 1.11
'    setting S-infinity equal to a little greater than SMAX to
'    prevent the possibility of logs of negative numbers and we know S-infinity
'    should be greater than SMAX
PRINT "Corr        S-infinity"
   QUE=0
VOCESUM:
A#=0 : B#= 0 : C#= 0 : D#= 0 : E#= 0 : F#= 0 : G#= 0 : J=0 'initialize variables to zero
REM*******
REM** Any changes to this area must also be changed below in the similar areas
REM*******
FOR I= STARTPT TO STOPPT
   J= J +1        'counter
   A#= A#+ STRAIN(I)        'sum of strains
      B0= LOG(SINF - STRESS(I))
   B#= B#+ B0        'sum of the dependent variables
   C#= C#+ (STRAIN(I) * B0)   'sum of the products
   D#= D#+ STRAIN(I)^2    'sum of the squared strain
   F#= F#+ B0^2     'sum of the squared dependent variable
NEXT I
   E#= A#^2
   G#= B#^2
R= ((J*C#) - (A#*B#))/SQR(((J*D#)- E#)*((J*F#)- G#))        'correlation
'*********************************************************
PRINT USING "+.#####     ###.##"; R,SINF
   IF ABS(R) >= CORR THEN    'have found a correlation which is higher
```

```
      CORR= ABS(R)              'save that correlation as the new one to beat
     IF CORR >= CORRMAX THEN
        CORRMAX= CORR    'save highest correlation
        SINF0= SINF          'save corresponding value of S-infinity
      END IF
      SINF= SINF+ STP       'increment S-infinity by some step size
      GOTO VOCESUM        ' return to summing and calc routines
   ELSEIF ABS(R)<CORR THEN
      QUE= QUE + 1
      IF QUE < 1  THEN
         SINF= SINF +STP
       GOTO VOCESUM
      ELSEIF QUE >= 1 THEN
         IF STP <= .1 THEN GOTO PUNCHOUT         'Escape from the loops
         QUE= 0
         SINF= SINF0 - STP 'go back two full steps before the max value of SINF
         STP=STP/10          'decrease the step size
         CORR=0
       GOTO VOCESUM
      END IF
   END IF
'************************************************************
PUNCHOUT:
'
REM** By now we should have the straightest line value of S-infinity so the
REM** slope of this line is the Voce coefficient, A, we will call it M.  The
REM** intercept is So.  NEED TO RECALCULATE THE SUMS OF THE LOG(...)
REM** BECAUSE THE MOST RECENT SET IS NOT THE STRAIGHT LINE SUM
REM** ANY CHANGES TO THE ABOVE SECTION MUST ALSO BE REFLECTED HERE
'
A#= 0 : B#= 0 : C#= 0 : D#= 0 : E#= 0 : F#= 0 : G#= 0 : J=0 : SINF= SINF0
'reinitialize variables
FOR I= STARTPT TO STOPPT
   J= J +1       'counter
   A#= A#+ STRAIN(I)
      B0= LOG(SINF - STRESS(I))
   B#= B#+ B0
   C#= C#+ (STRAIN(I) * B0)
   D#= D#+ STRAIN(I)^2
   F#= F#+ B0^2
NEXT I
   E#= A#^2
   G#= B#^2
R= ((J*C#) - (A#*B#))/SQR(((J*D#)- E#)*((J*F#)- G#))        'correlation
REM    We now calculate the straight line slope (M) and intercept for this value of
REM    S-infinity.  The intercept is the quantity (S-infinity - So) which we will
REM    call SINTER, S0 is approximately the 0.1% yield strength.
'
```

```
    M= ((J*C#)-(A#*B#))/((J*D#)-E#)
    M1= -1/M        'This is required because Voce takes the slope of the line where
            ' Strain is plotted on the Y-axis and log(Sinf - S) is on the X-axis...the
            ' reciprocal of what this program has done since stress is usually plotted
            ' on the Y-axis.  Where this 'line' crosses the stress axis is the location
            ' of S-infinity.  This value of the (negative) slope is called the
            ' characteristic strain.
    SINTER= (B#/J)-(M*(A#/J))
    S0= -(EXP(SINTER) - SINF0)
    BEEP
  PRINT
  PRINT
  PRINT "In the file " DAT$
  PRINT "Using the true stress and true strain:"
  PRINT
  PRINT "The Voce equation: S= Sinf - (Sinf-So)e ^-(E/A) ; where E is the strain"
  PRINT "Between points ";STARTPT;" and ";STOPPT;" of file ";DAT$
  PRINT "Has the coefficients:       Sinf= "SINF0"    So= "S0"     A= "M1
  PRINT "With a correlation of: "R
  PRINT "Necking begins at point "; MAXLODPT; " where the load is "; MAXLOD
  PRINT
  PRINT
  PRINT "Do you want a printout of the results (Y or N):";
    BEEP
    INPUT ANS$
    IF ANS$= "Y" OR ANS$= "y" THEN
      GOTO PRINTOUT
    ELSE
      GOTO RESTART
    END IF
  PRINTOUT:
    LPRINT
    LPRINT
    LPRINT "In the file " DAT$
    LPRINT "Using the true stress and true strain:"
    LPRINT
    LPRINT "For the Voce equation: S= Sinf - (Sinf-So)e ^-(E/A) ; where E is the strain"
    LPRINT "Between points ";STARTPT;" and ";STOPPT;" of file ";DAT$
    LPRINT "Has the coefficients:       Sinf= "SINF0"    So= "S0"    A= "M1
    LPRINT "With a correlation of: "R
    LPRINT "Necking begins at point "; MAXLODPT; " where the load is "; MAXLOD
    LPRINT
    LPRINT
    LPRINT CHR$(12)
  RESTART:
    PRINT
    PRINT
    PRINT "Do you want another run of this data set (Y or N):"
```

```
   PRINT "Select N if you had a bad data input and Y for the next question";
      BEEP
      INPUT A$
   IF A$= "Y" OR A$= "y" THEN GOTO BEGINNING
   PRINT
   PRINT "Do you want to run the program on another data file (Y or N):";
      BEEP
      INPUT A$
   IF A$= "Y" OR A$= "y" THEN GOTO NEXTFILE
END
```

APPENDIX C

BASIC Computer Program For Fitting an Exponential Function

```
REM** THIS PROGRAM IS TO TAKE TEMP/S0/S∞ DATA FROM A DATA
REM**  FILE, PUT IT INTO ARRAYS AND THEN CALCULATE THE EQUATION
REM**  COEFFICIENTS.
REM**
REM**  This program is written for the Apple Macintosh PC in Microsoft BASIC
REM** Version 3.0
'*************************************************************
REM
REM** DIMENSIONING THE CALCULATION ARRAY AND INPUT OF DATA
DIM TEMP(50) , S(50)
NEXTFILE:
PRINT
PRINT
PRINT "Input the name of your input file name with the Temp(°C)/S∞ or So"
PRINT "data in it.  The data should be in the same order "
PRINT
PRINT "INPUT FILE NAME:";
   BEEP
   INPUT DAT$
OPEN DAT$ FOR INPUT AS #1
PRINT
PRINT
N=0
REM**   LOOP THROUGH TO STORE TEMP/S∞ or S0 DATA IN ARRAYS FOR FUTURE
REM**   CALCULATIONS
   WHILE NOT EOF(1)
      N= N+1
      INPUT#1,TEMP(N) , S(N)
      TEMP(N)= TEMP(N)+273      'convert °C to °K
   WEND
CLOSE #1
REM
AGAIN:
PRINT N;" sets of data have been read from file "; DAT$
PRINT
PRINT "Enter the range of points you desire to look at using data point numbers"
PRINT "  separated by a comma.";
   BEEP
INPUT STARTPT,STOPPT
PRINT
```

```
PRINT "Sums of the data are now being calculated for a best correlation fit."
PRINT
PRINT
REM    For the calculation of sums the following notations will be used:
REM    stress coefficients = Y, Exp(Tc/T) = X,
REM     ΣX = A# , ΣY = B#, ΣXY = C#, ΣX^2 = D#, (ΣX)^2 = A#^2 = E#, ΣY^2 = F#,
REM     (ΣY)^2 = B#^2 = G# , R= correlation
REM
CORR= 0 : CORRMAX= 0 : STP= 10    'CORR and CORRMAX are a comparitive
'    correlation FOR use with R ; STP
'PRINT "Corr        TC"
   QUE=0
VOCESUM:
FOR TC= 1 TO 300
A#=0 : B#= 0 : C#= 0 : D#= 0 : E#= 0 : F#= 0 : G#= 0 : J=0 'initialize variables to zero
REM*******
REM** Any changes to this area must also be changed below in the similar areas
REM*******
FOR I= STARTPT TO STOPPT
   J= J +1        'counter
   A#= A#+ EXP(TC/TEMP(I))
   B#= B#+ S(I)
   C#= C#+ (S(I) * EXP(TC/TEMP(I)))
   D#= D#+ (EXP(TC/TEMP(I)))^2
   F#= F#+ (S(I))^2
NEXT I
   E#= A#^2
   G#= B#^2
R= ((J*C#) - (A#*B#))/SQR(ABS(((J*D#)- E#)*((J*F#)- G#)))        'correlation
'*********************************************************
   IF ABS(R) >= CORR THEN    'have found a correlation which is higher
      CORR= ABS(R)              'save that correlation as the new one to beat
     IF CORR >= CORRMAX THEN
        CORRMAX= CORR    'save highest correlation
        T0= TC           'save corresponding value of TC
      END IF
   END IF
NEXT TC
'*********************************************************
PUNCHOUT:
'
REM**  By now we should have the straightest line value of  TC so the
REM** slope of this line is the coefficient, C1, we will call it M.  The
REM** intercept is Co.  NEED TO RECALCULATE THE SUMS
REM** BECAUSE THE MOST RECENT SET IS NOT THE STRAIGHT LINE SUM
REM** ANY CHANGES TO THE ABOVE SECTION MUST ALSO BE REFLECTED HERE
'
A#= 0: B#= 0: C#= 0: D#= 0: E#= 0: F#= 0: G#= 0: J=0: TC= T0 'reinitialize variables
```

```
FOR I= STARTPT TO STOPPT
   J= J +1        'counter
   A#= A#+ EXP(TC/TEMP(I))
   B#= B#+ S(I)
   C#= C#+ (S(I) * EXP(TC/TEMP(I)))
   D#= D#+ (EXP(TC/TEMP(I)))^2
   F#= F#+ (S(I))^2
NEXT I
   E#= A#^2
   G#= B#^2
R= ((J*C#) - (A#*B#))/SQR(((J*D#)- E#)*((J*F#)- G#))        'correlation
REM    We now calculate the straight line slope (M) and intercept for this
REM    value of TC.  The intercept is the quantity C0
'
   M= ((J*C#)-(A#*B#))/((J*D#)-E#)
   C0= (B#/J)-(M*(A#/J))
   BEEP
PRINT
PRINT
PRINT "In the file " DAT$
PRINT "For an equation of the form:   S= Co + [C1*Exp(Tc/T)]"
PRINT
PRINT "The coefficients are:"
PRINT "          Tc= "T0"    Co= "C0"     C1= "M
PRINT "With a correlation of: "R
PRINT
PRINT
RESTART:
   PRINT
   PRINT
   PRINT "Do you want another run of this data set (Y or N):"
   PRINT "Select N if you had a bad data input and Y for the next question";
      BEEP
      INPUT A$
   IF A$= "Y" OR A$= "y" THEN GOTO AGAIN
   PRINT
   PRINT "Do you want to run the program on another data file (Y or N):";
      BEEP
      INPUT A$
   IF A$= "Y" OR A$= "y" THEN GOTO NEXTFILE
END
```

LIST OF REFERENCES

1. Enclopedia of Materials Science and Engineering, Bever, M.J., Volume 3, pp. 2157-2162, The MIT Press, 1986.

2. Metals Handbook Desk Edition, American Society for Metals, 1985.

3. Miglin, M.T. , Hirth, J.P. , Rosenfield, A.R. , Clark, W.A.T., "Microstructure of a Quenched and Tempered Cu-Bearing High-Strength Low-Alloy Steel," Metallurgical Transactions, pp. 791-798, Volume 17A, May 1986.

4. Wilson, E.A. , "Copper Maraging Steels," Journal of The Iron and Steel Institute, pp. 164-168, February 1968.

5. LeMay, I. , Krishnadev, M.R. , "The Economic Exploitation of High-Strength Low-Alloy Steels: Some Recent Developments," Paper presented at Interamerican Conference on Materials Technology, pp. 445-449, August 14-17, 1972.

6. Metals Handbook, Ninth Edition, Properties and Selection: Irons and Steels, American Society for Metals, Volume 1, 1978.

7. Coldren, A.P. and Cox, T.B. , DTNSRDC report. , SME-CR-07-86, July 1986.

8. Vassilaros, M.G. and Natishan, M.E. , "Micromechacics of Brittle and Ductile Crack Initiation and Growth," DTNSRDC private communications.

9. Tegart, W.J. McGregor , Elements of Mechanical Metallurgy, The Macmillan Company, 1967.

10. Meyers, M.A. , Chawla, K.K., Mechanical Metallurgy, Principals and Applications, Prentice-Hall, 1984.

11. Conway, J.B. , Stentz, R.H. , Berling, J.T. , Fatigue, Tensile, and Relaxation behavior of Stainless Steels, Technical Information Center, Office of Information Services, United States Atomic Energy Commission, 1975.

12. Voce, E. , "A Practical Strain Hardening Function," Metallurgia , pp. 219-226, Volume 51, May 1955.

13. Bridgman, P.W. , Studies in Large Plastic Flow and Fracture, pp.9-37, McGraw-Hill, 1952.

14. Hamilton, J.E. , The Effect of Temperature on the Tensile Properties of HSLA-100 Steel, Master's Thesis, Naval Postgraduate School, Monterey, California, June 1987.

INITIAL DISTRIBUTION LIST

		No. Copies
1.	Defense Technical Information Center Cameron Station Alexandria, Virginia 22304-6145	2
2.	Library, Code 0142 Naval Postgraduate School Monterey, California 93943-5002	2
3.	Department Chairman, Code 69Hy Department of Mechanical Engineering Naval Postgraduate School Monterey, California 93943-5000	1
4.	Professor K. D. Challenger, Code 69Gh Department of Mechanical Engineering Naval Postgraduate School Monterey, California 93943-5000	5
5.	Mr. M. G. Vassilaros, Code 2814 David W. Taylor Naval Ship R&D Center Annapolis, Maryland 21402	2
6.	Commander, Naval Sea Systems Command Attn: Mr. Charles Hull, Code 05 Naval Sea Systems Command Headquarters Washington , D.C. 20362-5101	1
7.	Commander, Naval Sea Systems Command Lcdr. W. Elger, Code 05M Naval Sea Systems Command Headquarters Washington , D.C. 20362-5101	1
8.	Dr. J. Gudas, Code 2800 David W. Taylor Naval Ship R&D Center Annapolis, Maryland 21402	1
9.	Mr. T. Kellog, Code 69 Department of Mechanical Engineering Naval Postgraduate School Monterey, California 93943-5000	1

10.	Mr. Mauro Losz, Code 69Lo Department of Mechanical Engineering Naval Postgraduate School Monterey, California 93943-5000	1
11.	Lt. David M. Bissot 25 Deer Run Rd. Little Baltimore Newark, Delaware 19711	5

Thesis
B5452695 Bissot
c.1 Development of a constituitive equation for HSLA-100 at cryo-genic temperatures.